Science of the Total Environment 763 (2021) 144444

Contents lists available at ScienceDirect

Science of the Total Environment

journal homepage: www.elsevier.com/locate/scitotenv

Whole-island wind bifurcation and localized topographic steering: Impacts on aeolian dune dynamics

Alex Smith [a,*], Derek W.T. Jackson [b,c], J. Andrew G. Cooper [b,c], Meiring Beyers [d], Colin Breen [b]

[a] School of the Environment, University of Windsor, Windsor, Ontario N9C 2J9, Canada
[b] School of Geography and Environmental Science, Ulster University, Coleraine, UK
[c] Geological Sciences, School of Agricultural, Earth and Environmental Sciences, University of KwaZulu-Natal, Westville Campus, Durban, South Africa
[d] Klimaat Consulting & Innovation Inc., 49 Winston Cr, Guelph, Ontario N1E 2K1, Canada

HIGHLIGHTS

- Whole-island airflow bifurcation and topographic steering occurs around a dunefield.
- Inconsistency in regional wind patterns and dune migrations rates were observed.
- Meteorological observations, wind modelling, and remote sensing data were compared.
- Incident winds are perturbed, modifying aeolian transport patterns at the dunefield.
- Down-scaling winds may better predict dominate drivers in aeolian environments.

GRAPHICAL ABSTRACT

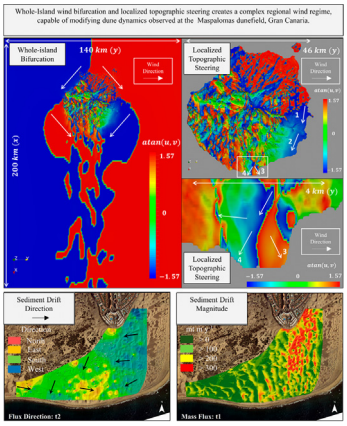

ARTICLE INFO

Article history:
Received 28 September 2020
Received in revised form 24 November 2020
Accepted 8 December 2020
Available online xxxx

Editor: Fernando A.L. Pacheco

Keywords:
Dunes
Aeolian
Computational fluid dynamics (CFD)
Remote sensing

ABSTRACT

Topographic steering has been observed around Gran Canaria, a high-profile circular island located in the Canary Island Archipelago, Spain, culminating in a complex lee-side wind regime at the Maspalomas dunefield. Maspalomas has experienced rapid environmental changes since the 1960s, coincident with a boom in the tourism industry in the region and requires further examination on the linkages between meso-scale airflow patterns and aeolian processes modifying the landscape. The aim of this work is to simulate mean and turbulent airflow conditions at Maspalomas due to incremental changes in the regional wind direction and to compare these results to the predicted and observed aeolian dynamics taken from meteorological records, a global wind retro-analysis model, and remote sensing data. A Smagorinsky Large Eddy Simulation (S-LES) model was used to identify meso-scale airflow perturbations and turbulence at different locations around the island. Variability in meteorological data was also identified, with sites recording accelerated or retarded velocities and directional distributions ranging between unimodal to bimodal. Using a global retro-analysis model, relatively consistent upwind conditions were predicted over a period coinciding with three aerial LiDAR surveys (i.e., 2006, 2008, and 2011) at the Maspalomas dunefield. Despite the consistent predicted airflow conditions, dune migration rates dropped from 7.26 m y^{-1} to 2.80 m y^{-1} and 28% of dunes experienced crest reversal towards the east, or opposite of the primary westerly migration direction during the second time period. Our results indicate that meso-scale airflow steering alters local wind conditions that can modify sediment transport gradients at Maspalomas. Given the rapidity of environmental changes and anthropogenic impacts at Maspalomas, these findings improve our

* Corresponding author.
E-mail address: absmith9@uwindsor.ca (A. Smith).

https://doi.org/10.1016/j.scitotenv.2020.144444

understanding on the aeolian dynamics at Maspalomas and can be used to inform future management strategies. Lastly, the approach used in this study could be applied to other high-profile island settings or similarly complex aeolian environments.

1. Introduction

The bedforms and landforms present in aeolian environments develop over a continuum of spatial (e.g., ripples to draas) and temporal (e.g., seconds to millennial) scales (Wilson, 1972); however, linking our understanding of the hierarchical network of processes working at each scale is difficult (Walker et al., 2018). Problems arise when attempting to up- or down-scale aeolian processes, as in other geomorphological systems, and depends primarily on the scale of interest and objectives of the research, where certain variables are either dominant (primary geomorphic driver) or passive (not relevant) at each specific scale (de Boer, 1992). For example, dominant micro-scale variables (i.e., <2 km and ranging from seconds to hours) can include rapid turbulence fluctuations and form-flow interactions; however, at the meso-scale (i.e., >2–2000 km and ranging from days to months) these may become passive (Orlanski, 1975). In the latter case, the prevailing regional wind conditions could become dominant due to the larger spatial and temporal scales operating on the system. Despite this discontinuity, the landforms occurring within aeolian systems are the result of processes working at all scales, and therefore require a more holistic approach to understanding emerging patterns in aeolian landscapes (de Boer, 1992).

Since the early 2000s, advances and accessibility of field sensors have allowed aeolian research to focus on landform, or micro-scale studies, that have measured high-resolution three-dimensional turbulent airflow (Jackson et al., 2011; Lee and Baas, 2012; Chapman et al., 2012, 2013; Smyth et al., 2012, 2013, 2014; Delgado-Fernandez et al., 2013a; Hesp et al., 2013; Smith et al., 2017a) coupled sediment transport patterns (Baddock et al., 2011; Weaver and Wiggs, 2011; Wiggs and Weaver, 2012; Baas et al., 2020), and resultant topographic change (Delgado-Fernandez et al., 2018; Cornwall et al., 2018a, 2018b). Contemporaneously, attempts to capture meso-scale dynamics have been less common but have included physical (Bullard et al., 2000; Garvey et al., 2005), conceptual (Delgado-Fernandez and Davidson-Arnott, 2011), and numerical models (Hernández-Calvento et al., 2014; Smith et al., 2017b) and in-situ field studies (Wiggs et al., 2002; Jackson et al., 2013a; Delgado-Fernandez et al., 2011, 2013a), demonstrating the modification of regional airflow conditions and the impact on aeolian landforms. Despite advances in our understanding of both micro- and meso-scale aeolian processes, there remains practical limitations on the spatial and temporal scales that can be monitored (Bauer et al., 2013). Another emergent research methodology, computational fluid dynamics (CFD), can overcome some of these limitations because models are fully scalable and allow for characteristic form-flow relationships to be simulated across a range of surface roughness elements and aeolian bedforms, landforms, and landscapes (Parsons et al., 2004a, 2004b; Pelletier, 2009; Jackson et al., 2011, 2013a, 2013b, 2020; Smyth et al., 2012, 2013, 2014, 2019, 2020; Smyth, 2016; Hesp et al., 2015; Hesp and Smyth, 2016, 2019; Smith et al., 2017a, 2017b; Zhao et al., 2019). These studies have demonstrated the utility of CFD to simulate and identify complex flow patterns affecting aeolian environments at multiple scales.

1.1. Regional setting and research objectives

Pronounced meso-scale (10s km) topographic steering and coherent turbulent flow structures (e.g., von Kármán vortex streets, VKVS) can be observed downwind of the Canary Island Archipelago, where remotely sensed images of the cloud cover are able to capture vortex shedding phenomena (Fig. 1A; (Conover, 1964; Zimmerman, 1969; Jensen and Agee, 1978; Etling, 1989)). Around the island of Gran Canaria, significant topographic steering has been recorded in field studies that have observed airflow deflection around the island, parallel to the coastline, and the development of turbulent eddies in the lee (Barton et al., 2000; Basterretxea et al., 2002). Despite this evidence of meso-scale controls, it is still not well understood how topographic steering modifies localized wind conditions around the island's coastline. As a result, a reliance on regional meteorological data may not adequately describe the competent wind regime responsible for local aeolian dynamics, particularly in turbulent lee-side locations such as the Maspalomas dunefield.

The migration of barchan dunes at Maspalomas is primarily controlled by NE Trade Winds that are topographically steered towards the east around the island's massif (Nadal and Guitián, 1983; Martínez et al., 1986; Martínez, 1990; Naranjo, 1999; Hernández-Calvento, 2006), increasing in consistency and magnitude during the winter months (Máyer-Suárez et al., 2012). As regional wind conditions deviate towards N during the summer months, a distinct westerly airflow component can be observed at Maspalomas as winds become steered and accelerated around the higher relief western coastline (Viera-Pérez, 2015). Furthermore, opposing easterly and westerly airflow have been observed simultaneously within the dunefield and can fluctuate throughout the day (Hernández-Calvento, 2006; Máyer-Suárez et al., 2012). While thermally driven diurnal winds are thought to contribute in part to this variability (Máyer-Suárez et al., 2012), it is evident from these previous studies that significant topographic steering of northerly winds occurs around the high relief island topography, culminating in a complex lee-side wind regime at the Maspalomas dunefield.

Maspalomas has experienced rapid changes to the environment and wind patterns since the growth of the local tourism industry beginning in the 1960s (Hernández-Calvento et al., 2014; García-Romero et al., 2016, 2019a, 2019b; Hernández-Cordero et al., 2017, 2018; Smith et al., 2017b), requiring new management practices to monitor the changing ecological and deflationary patterns within the dunefield (Hernández-Cordero et al., 2006). Meso-scale airflow models have previously been developed for the region to predict wind speed, direction, and turbulence intensity based on the island topography and terrain roughness (i.e., developed by the Canary Island Technological Institute (ITC); https://www.grafcan.es/2014/01/el-mapa-eolica-en-idecanarias) and urban development (Hernández-Calvento et al., 2014). Alternatively, CFD models can be used to improve simulations particularly of topographically induced flow perturbations and turbulence (e.g., Smyth, 2016). Smith et al. (2017b) used a meso-scale CFD model to identify the influence of progressive stages of urbanization at Maspalomas. Distinct zones of velocity acceleration (i.e., increased erosivity) and deceleration (i.e., decreased erosivity) were identified, corresponding to landcover changes in the dune field through time. Given the complexity of the local wind regime and significant environmental changes occurring at Maspalomas, further examination of the linkages between meso-scale airflow and aeolian dynamics are required and can ultimately be used to inform future management strategies.

In this study we use a CFD model to simulate and describe meso-scale controls on regional topographic steering, examine the potential impact on dune dynamics at Maspalomas, and present further considerations of modelling airflow conditions in complex aeolian environments. The primary objectives of this study are to: (1) Overview airflow conditions

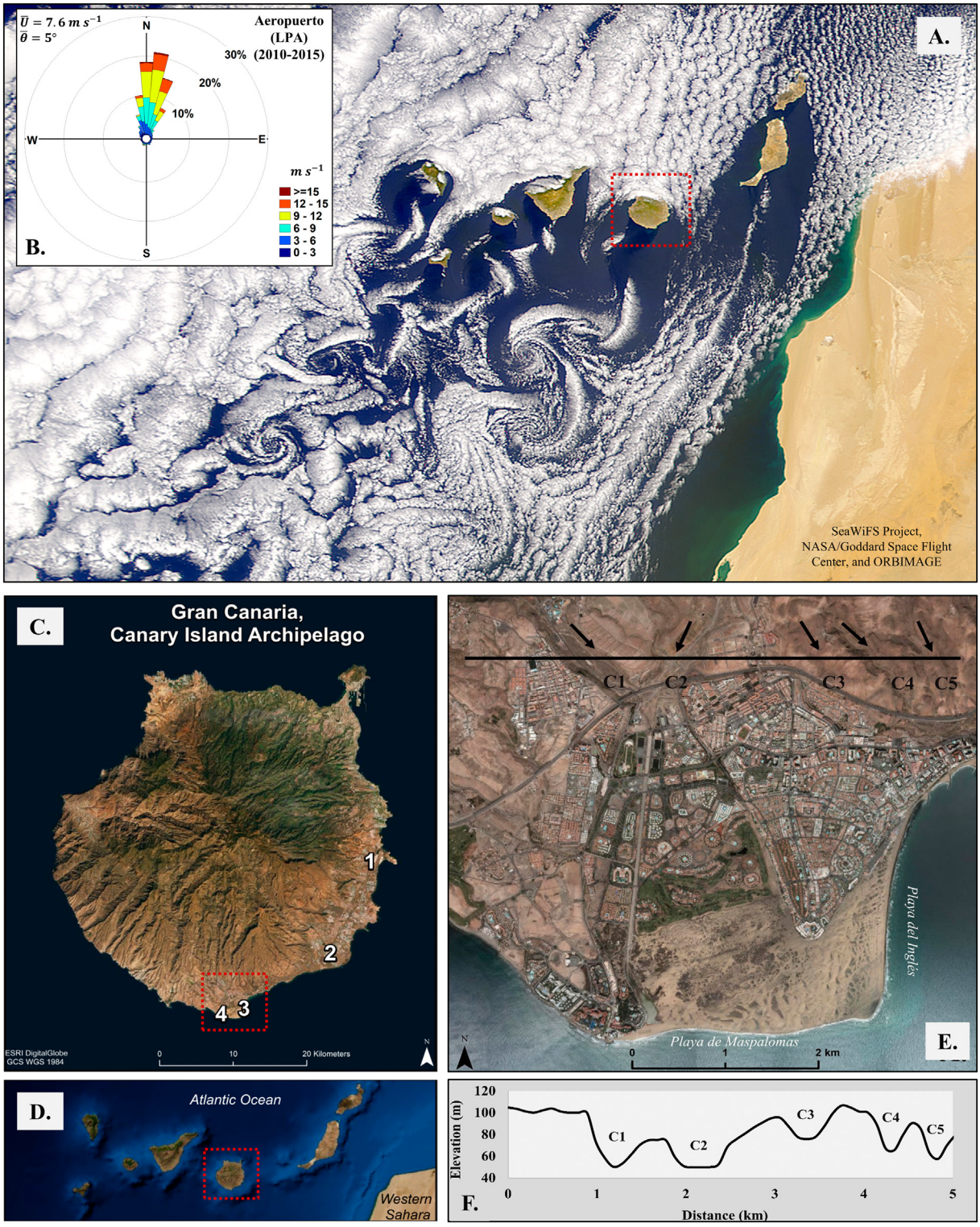

Fig. 1. During frequent NE Trade Winds, meso-scale topographic steering in the form of VKVS can become visible in the cloud layer downwind as turbulent vortices are shed off of the Canary Island Archipelago, located ~230 km off the coast of Morocco and Western Sahara (A, B; SeaWifs Project, NASA/Goddard Space Flight Center, and ORBIMAGE). The primary wind regime for Gran Canaria (C,D), recorded at Las Palmas Airport (Aeropuerto), is unimodal with northerly winds predominating throughout the year (B, C.1). Other meteorological stations record significant flow perturbations including retarded and deflected winds at El Matorral (C.2) and bimodal wind conditions at Inglés (C.3) and Maspalomas (C.4). At the lee-side Maspalomas dunefield (E), barchan and barchanoid dune ridges migrate primarily from the NE to SW, although significant intra-site variability has been observed within the dunefield. Meso-scale (A) and local airflow perturbations from urbanization and canyon topography (E, F) creates a complex wind environment at Maspalomas.

recorded by regional meteorological stations, (2) Present topographically-forced regional airflow perturbations using CFD modelling, (3) Quantify remotely sensed dune mobility (i.e., direction and magnitude of migration and sediment flux) occurring through time, and (4) Discuss inconsistencies between measured and modelled regional airflow patterns and observed dune dynamics. While this work offers an insight into conditions unique to the Maspalomas dunefield, it also

highlights general considerations for modelling regional boundary conditions for research in aeolian geomorphology.

2. Study site

2.1. Gran Canaria

Gran Canaria (27°56′ N and 15°35′W) is a 1532 km^2 semi-circular volcanic island, located ~230 km off the west coast of Morocco and Western Sahara, in the Canary Island Archipelago, Spain (Fig. 1A,C, D; (Acosta, et al., 2003)). The island is ~45 km in diameter and reaches a maximum elevation of 1949 m above mean sea level (MSL; (Acosta, et al., 2003)). From the island interior, a network of canyon systems, known as 'barrancos', extend radially outward to the coastline (Fig. 1C; (Funck and Schmincke, 1998; Acosta et al., 2003)). Given the position of the Canary Islands, relative to the Azores High Pressure system in the mid-Atlantic, NE Trade winds predominate as the Coriolis Effect deflects winds towards the equator (Fernandopullé, 1976). The Agencia Estatal de Meteorología (AEMET) station at the Las Palmas Airport is the primary meteorological station on the island, reporting unimodal northerly winds with an average direction ($\bar{\theta}$) of 5° and an average velocity ($\bar{U}$) of 7.6 m s^{-1} between 2010 and 2015 (Fig. 1B). During consistent northerly Trade Winds, meso-scale airflow perturbations in the form of VKVS can develop downwind of the Canary Islands (Fig. 1A). A capping inversion layer below the obstacle height (i.e., island topography) is an important driver in the development of VKVS as flow is deflected laterally around the island rather than over (Nunalee and Basu, 2014).

2.2. Maspalomas dunefield

Maspalomas (27°44′ N and 15°34′ W; Fig. 1F) is a ~ 3.6 km^2 arid dunefield located on southern coast of Gran Canaria (Fig. 1C,E). Sediment is supplied from the nearshore onto the eastern beach face at Playa del Inglés (Martínez et al., 1986; Hernández-Calvento, 2006; Bouzas et al., 2013). Competent NE winds exceeding the sediment threshold ~5.5 m s^{-1} mobilizes sediment, ranging between 0.18 and 0.22 mm in diameter, towards the SW terminus at Playa de Maspalomas with average dune migration rates between ~5 to 8 m y^{-1} (Pérez-Chacón Espino et al., 2007; Máyer-Suárez et al., 2012; Smith et al., 2017a). Despite this general migration path, a distinct bimodality in wind conditions have been recorded at Maspalomas (e.g., Viera-Pérez, 2015). Barchan dunes, adjacent to Playa del Inglés, can migrate up to 35 m y^{-1} before coalescing into barchanoid ridges in the central section of the dunefield (Hernández et al., 2007; Pérez-Chacón Espino et al., 2007; Jackson et al., 2013b). As wind energy and sediment supply decrease westward (Smith et al., 2017a), individual barchan dunes re-emerge in the terminus section of the dunefield adjacent to Playa de Maspalomas (Fig. 1E). These barchan dunes have distinct morphology including rounded crest and brinklines, truncated arms, and slower migration rates (Martínez et al., 1986; Hernández-Calvento, 2006; Pérez-Chacón Espino et al., 2007; Hernández-Cordero et al., 2015; Smith et al., 2017a, 2017b).

Steep canyon topography is located ~3 km north of the Maspalomas dunefield, including five channels with an average width of ~640 m (Fig. 1F,E). Northwest of the dunefield, two wider channels (i.e., C1 and C2) converge before opening on to a progressively sloping alluvial plane that extends south to Playa de Maspalomas. Three narrower channels (i.e., Cs 3–5), located northeast of Maspalomas, are directed to the southeast and terminate north of the urban area or extend towards the shoreline north of Playa del Inglés. While the urban area and dune landforms have been show to modify approaching wind conditions (Hernández-Calvento et al., 2014; Smith et al., 2017b; García-Romero et al., 2019b), the adjacent canyon topography may additionally perturb winds approaching the dunefield (e.g., Máyer-Suárez et al., 2012) and will be explored further in this study.

3. Methodology

3.1. CFD Modelling

To reproduce characteristic airflow steering around Gran Canaria, CFD wind modelling was conducted in OpenFOAM, an open source CFD modelling software (https://openfoam.com/). The pisoFoam solver was used to implement the Smagorinsky Large Eddy Simulation (S-LES) model (Smagorinsky, 1963). LES allows for the turbulent fluctuation of airflow conditions to be monitored through time, as opposed to steady state solvers that run until the model variables reach an acceptable level of convergence (e.g., $k-\varepsilon$ and *RNG* $k-\varepsilon$; Smith et al., 2017a). An approaching freestream velocity (U (m s^{-1})) profile was mapped at the model inlet, using the Hellmann (1916) 'power law' velocity profile (Eq. (1)).

$$U = U_r\left(\frac{Z}{Z_r}\right)^{\alpha} \tag{1}$$

where (U_r (m s^{-1})) represents the reference velocity taken from the reference height (Z_r (m)), (Z (m)) is the variable height above the surface, and (α) is a model constant taken as 0.16. For the S-LES model, the sub-grid scale eddy viscosity (*nuSGS* (m^{2}s^{-1}; Eq. (2)) was determined across the model surface, taken as:

$$nuSgs = C_k\sqrt{k}\Delta \tag{2}$$

where (C_k) is a model constant 0.094, (k (m^{2}s2)) is the turbulent kinetic energy, and (Δ (m^3); Eq. (3)) is the cell volume.

$$\Delta = Kz\left[1-\exp\left(-\frac{z^+}{A}\right)\right] \tag{3}$$

Here we use the sub-grid van Driest damping function (Van Driest, 1956) for Δ in order to model turbulence in the near wall viscous sub layer with (K) representing the von Kármán's constant taken as 0.4187 which is standard for the S-LES model, (z (m)) representing the distance from the model wall, (z^+; Eq. (4)) is the dimensionless wall unit, and (A) is a model constant of 26.

$$z^+ = zu_*/v \tag{4}$$

Here, (u_* (m s^{-1}); Eq. (5)) is the shear velocity and (v (m^2 s^2) is the kinematic viscosity which is ~1.5 x $-$ 10^5 for air temperatures at 20 °C.

$$u_* = \sqrt{\frac{\tau_\omega}{\rho}} \tag{5}$$

where (τ_ω (*Pa*); Eq. (6)) is the wall shear stress and (ρ (kg m^3)) is the density of air.

$$\tau_\omega = \mu\frac{\partial u}{\partial z_{z=0}} \tag{6}$$

Here, (μ (*Pa s*); i.e., *p x v*) is the dynamic viscosity and (u (m s^{-1})) is the streamwise velocity. A turbulent wall function was included by specifying roughness values, where zero gradient conditions occur. The roughness height ($K_{s,\ ABL}$(m); Eq. (7)) were given a constant value of 15 for an aerodynamic roughness length z_o=0.5 m for the island topography and 0.006 over open sea with z_o=0.0002 m, corresponding to roughness constants $C_{s,\ ABL}$ (m); Eq. (8)) of 0.32 for both the open ocean and island topography (Troen and Petersen, 1989; Blocken et al., 2007).

$$K_{s,ABL} = 30z_o \tag{7}$$

$$C_{s,ABL} = (9.73/K_{s,ABL})z_o \tag{8}$$

Roughness values used for this study were generalized (i.e., constant for terrain and ocean surfaces) due to the large computational costs requiring some simulation generalizations.

Model simulations were run for three incident wind directions including NNE (Case 1), N (Case 2), and NNW (Case 3), chosen to represent the incremental changes to the characteristic unimodal northerly wind regime recorded at Aeropuerto (Fig. 1B). Each case maintained an inlet 'power law' velocity (Eq. (1)) of 10 m s^{-1} at 500 m (z), corresponding to the yearly $\overline{U}$ of 7.3 m s^{-1} at 10 m (z) recorded at Aeropuerto. The model domain dimensions for each simulation were 200 km (x) - 140 km (y) - 10 km (z). The island topography is located ~27 km downwind of the model inlet and, due to the large extent of the model domain, cells located away from the island topography had a consistent size of 1 km (x) x 1 km (y) x 1 km (z). Four levels of progressive mesh refinement were specified for cells near the island topography with maximum refinement of 180 m (x) - 90 m (y) - 107 m (z) at the surface. Overall, the model domain had a total of 1.6×10^6 cells for each simulation. The island topography was rotated within the mesh depending on the orientation of the initial flow conditions (i.e., 0 ° ± 22.5°) for cases 1–3. Simulations were run with a conservative time step (δt) of 2.5 s in order to satisfy the Courant-Friedrichs-Lewy condition (Courant et al., 1928), maintaining a Courant number (Co; Eq. (9)) less than one:

$$Co = \frac{\delta t |U|}{\delta x} \tag{9}$$

where U is the magnitude flow velocity (Eq. (10)) and δx is the cell size in the direction of the flow velocity. For example, given values of $\delta x = 90$ m (y-direction) and $\delta t = 2.5\,s$, you would require $U \leq 36$ m s^{-1} to satisfy Eq. (6). Maintaining $Co < 1$ throughout the model run ensures accurate and stable simulations as model calculations have sufficient time to transfer flow conditions to adjacent cells. Each model was run for a total simulation period of 30 h with the first 6 h excluded from the analysis to allow ABL conditions to fully develop over the model domain in the x-direction. Results Therefore, results present data sampled at each site location (i.e., 1–4) during a 24-h simulation period for each incident flow angle (i.e., Cases 1–3).

3.2. Model sampling

Instantaneous values for flow velocity (U (m s^{-1}); Eq. (10)) and flow direction (θ (°); Eq. (11)) were determined from the three-dimensional flow vectors (e.g., Delgado-Fernandez et al., 2013a), sampled at four study sites (i.e., Aeropuerto, El Matorral, Inglés, and Maspalomas; see Section 4.1) at a height of 50 m (z) above the island model surface.

$$U = \sqrt{u\prime^2 + v\prime^2 + w\prime^2} \tag{10}$$

$$\theta = \theta_r - \left(atan2(u, v)\left(\frac{180}{\pi}\right)\right) \tag{11}$$

Here, (u, v, w (m s^{-1})) are the streamwise, spanwise and vertical flow vectors and (θ_r) is the rotation in degrees of the island surface (i.e., 22.5° for Case 1, 0° for Case 2, and 337.5° for Case 3). Time variant three-dimensional flow vectors were then used to measure the dimensionless turbulence intensity (TI; Eq. (12)), where (k (m^2 s^2); Eq. (13)) is the turbulent kinetic energy and ($\overline{U}$ (m s^{-1})) is the average wind velocity taken during the 24-h sample period (Jackson et al., 2011; Smyth et al., 2013, 2014).

$$TI = \frac{\sqrt{\frac{2}{3}k}}{\overline{U}} \tag{12}$$

$$k = \frac{1}{2}\left(\sigma_u{}^2 + \sigma_v{}^2 + \sigma_w{}^2\right) \tag{13}$$

The variability in θ among instantaneous data samples (i) was identified by the consistency index (C_I; Eq. (14); (Heidorn, 1978)), taken as:

$$C_I = \frac{100}{n}\sqrt{\left[\left(\sum_i^n sin\,\theta_i\right)^2 + \left(\sum_i^n cos\,\theta_i\right)^2\right]} \tag{14}$$

where (n) is the total number of samples. Jackson and Hunt's (1975) speed-up perturbation ratio (U_δ (%); Eq. (15)) normalised $\overline{U}$ to upwind conditions by the average incident or unperturbed flow (i.e., $\overline{U_I}$) at the same height (i.e., 50 m).

$$U_\delta = \left(\frac{\overline{U} - \overline{U_I}}{\overline{U_I}}\right)100 \tag{15}$$

Similarly, a directional perturbation ratio (θ_Δ (%); Eq. (16)) normalised the mean directionality ($\overline{\theta}$) to mean upwind directionality (i.e., $\overline{\theta_I}$), to determine the magnitude of flow deflection at each study site (i.e., −50–50%).

$$\theta_\Delta = \left(\frac{\overline{\theta} - \overline{\theta_I}}{360}\right)100 \tag{16}$$

3.3. Dune dynamics

3.3.1. Global wind retro-analysis and sand drift potential

Discontinuity in the available regional data for Gran Canaria represented a significant challenge in identifying the airflow patterns responsible for modifying dunes at Maspalomas. To address these data gaps, a retrospective analysis of regional airflow patterns was obtained from NASA's Prediction of Worldwide Energy Resources (POWER) dataset. This provided daily airflow direction and speed at 10 m above the ocean surface in an obstructed location ~22 km upwind of Gran Canaria (28°20′ N, 15°34′ W), covering the intervening periods between successive LiDAR surveys used to monitor dune dynamics from 2006 to 2008 and 2008–2011. The historical regional wind conditions were generated from NASA's Modern Era Retro-analysis for Research and Applications (MERRA−2) assimilation model that has a global grid resolution of 0.5° x 0.5°. The MERRA-2 model offers a range of research applications (e.g., Gelaro et al., 2017), including a recent example in aeolian research (Madurapperuma et al., 2020).

Coastal and desert dune research has often implemented the "Fryberger Model" (FM) (Fryberger and Dean, 1979) to describe the influence of regional airflow on the potential for sediment mobilization and the development of characteristic dune morphometry. Based on an equation by Lettau and Lettau (1978), the mass flux rate (q (kg m s^{-1}); Eq. (17)) can be predicted, by:

$$q = C\sqrt{\frac{d}{D}}u_*{}^2(u_* - u_{*t})\frac{\rho}{g} \tag{17}$$

where C is a model constant taken as 6.7, d is the grain diameter of the study site, D is the reference grain diameter of 25×10^{-5} m, and u_{*t} is the fluid threshold shear velocity in m s^{-1}. The FM modifies q to provide a non-dimensional sediment flux potential (FMq; Eq. (18)):

$$FMq \propto U_Z{}^2(U_Z - U_{*Z})t \tag{18}$$

Here, (U_Z (m s^{-1})) is a weighted reference wind speed (i.e., taken as the mid-point of pre-defined velocity bins) and impact threshold (U_{*Z} (m s^{-1})) at height (Z (m)) above the surface, assuming that the shear velocity is proportional to wind velocity at a given height (Belly, 1964), and the duration of the record (t) expressed as a %.

FMq values, derived from our regional wind retro-analysis, were summed to predict the sand drift potential (DP) in dimensionless vector

units for a 16-point or 22.5° directional grouping (e.g., N, NNE, etc.). This study incorporates suggested modifications to the FM including using wind velocities and bins expressed in m s^{-1} (Bullard, 1997) and using the statistical mean for U_Z (Pearce and Walker, 2005). Additionally, the resultant vector (RDP) and direction (RDD) and the variability of the competent wind regime (RDP/DP) are reported. DP values are commonly used to describe the regional wind energy from low (<27), intermediate (27–54), and high (>54), following the conversion to winds recorded in m s^{-1} (Bullard, 1997). RDP indicates the overall magnitude of sand drift predicted in a given direction or DDP. Lastly, RDP/DP is the normalised variability of wind patterns, ranging from complex (approaching 0) to narrow unimodal (approaching 1).

3.3.2. Crest migration and mass flux analysis

Dune dynamics are often used as a proxy to assess regional airflow regimes (e.g., Smith et al., 2017c; Smyth et al., 2020) and are hereby used to examine the influence of predicted meso-scale airflow conditions. Remotely sensed dune migration patterns including celerity (c (m y^{-1})), or the rate of crest migration per year, and celerity direction (θ_c (°)) were measured from two time series of LiDAR-derived digital elevation models (DEMs). Time series 1 (t_1) represents changes taking place over a 498-day period between 10/22/2006–03/03/2008 and time series 2 (t_2) over a total of 1287 days between 03/03/2008–09/11/2011. The 2006 and 2008 LiDAR datasets were processed using the methods described in Vallejo et al. (2009), with a reported vertical accuracy of 0.05 m between surveys. The elevation values for the 2011 dataset were manually georeferenced using coincident pixels from the previous two DEMs, taken from highly stable deflationary zones within the dunefield (i.e., where little or no aeolian transport occurs) with the maximum error of ~0.20 m, relative to both the 2006 and 2008 datasets.

c and θ_c were measured with a semi-automated extraction technique proposed by Dong (2015) using an ArcGIS environment, with a general work flow that includes; 1. Conversion of a DEM to a degree-slope raster, 2. Generation of a binary raster capturing the slip face (i.e., 30° ≤ slope ≥ 35°), 3. Noise removal and vectorization of the slip face to centrelines, 4. Designation of a standard search radius through buffer generation, 5. Generating random points along the slipface centrelines, and 6. Calculating the distance and direction of the points to the nearest intersection of the previous slip face centreline, within the predefined search radius.

This technique was modified for this study due to the presence of crest reversals occurring in t_2 that resulted in the presence of slip faces on both the lee and upper stoss slopes. To account for the complexity of dune shapes between time series, c and θ_c were measured from the displacement of the crest positions between successive surveys. During step 2, as outlined above, the slope raster was used to create a standard deviation raster using a moving 3 × 3 window to identify significant breaks in slope, representing the boundary between the crest line and lee slope. A user defined threshold, with a slope standard deviation of ≥4, was used to extract the dune crestline, before continuing with steps 3–6. Given the extensive time period between surveys, it was critical to manually assess the dune forms sampled in this study and required the removal of measurements from dunes that display significant variability in shape (e.g., coalescence) or if uncertainty existed in dune identifications between time series.

Bagnold (1941) observed the relationship between c and dune height (H (m)) to provide the 'long period' mass flux (Q; Eq. (19)) estimate, given by:

$$cH = Q/\sigma \tag{19}$$

where, (σ) is the bulk density of the sand taken as 2650 kg m^3. Bagnold (1941) analyzed dune migration rates in relation to wind conditions over a five-year data set, monitoring the c of barchan dunes in the Kharga Oasis, Egypt (Beadnell, 1910). This method requires estimates of Q to be made over a uniform meteorological area (e.g., within a dunefield), and assumes that sediment transported over the dune crest is deposited on the stoss slope (i.e., conservation of mass during migration). Despite its relative simplicity, Q does provide a systematic and repeatable estimation of mass flux from monitored dune migration that can be derived from LiDAR datasets.

To predict the mass flux occurring between each time series, c and θ_c sampled across the dunefield, were used to create a celerity and directional raster using an Inverse Distance Weighted interpolation in ArcGIS. Furthermore, the deflationary basement elevation, identified as 2.6 m on average throughout the dunefield, was subtracted from the LiDAR DEMs and used to estimate the height of the active dune deposits above the non-erodible bed (H_d (m)). Given a littoral sediment deficit at Maspalomas (Bouzas et al., 2013) resulting in the progressive lowering of the dunes (Hernández et al., 2002, 2007), we take the H_d from the endpoint dune crest position from the latest DEM (i.e., 2008 for t1 and 2011 for t2) to provide a conservative estimate of elevation values in each series. Then by rearranging Eq. (19), we can obtain an estimation of mass flux (MF (mt m y^{-1}); Eq. (20)), taken as:

$$MF = \frac{cH_d\sigma}{n/365}0.001 \tag{20}$$

where n represents the number of days and the reported mass converted into metric tons for convenience. Similar to the FM described above, the average MF estimates signifies the energy of the dunefield over a given time series, RMF and DMF indicates the magnitude of flux expected in a resultant direction, and RMF/MF describes the variability of flux directions measured across the dunefield. Therefore, MF results can be compared to those obtained by the FM to identify how well dune dynamics at Maspalomas can be described by regional wind patterns.

4. Results

4.1. Recorded regional wind conditions

Four simultaneously recording meteorological stations were sampled including: 1. Aeropuerto; 2. El Matorral; 3. Inglés; and 4. Maspalomas (Figs. 1C and 2A,B,C,D). Averages for wind speed and directionality, taken during a ~ three-month 91 day period from 01/15/205 to 04/10/2015, were collated for each station (Fig. 2A,B,C,D). Averages represent hourly records for the Aeropuerto (96% data coverage), El Matorral (94% data coverage), and Maspalomas (76% data coverage) stations. The Inglés (83% data coverage) station recorded winds every 10 min which likely caused an increase in velocity range and in the directional bins, particularly the NW component (Fig. 2C), although the overall bimodal distribution agrees well with the nearest Maspalomas station (Fig. 2D), located ~3.5 km to the NW. A major challenge of this study was the absence or frequent gaps in the available meteorological station data and we were limited to this brief window to analyze concurrent wind conditions; however, the short-term airflow directions recorded at Aeorpuerto and Maspalomas agree well with longer term distributions (Fig. 1B; (Smith et al., 2017a)), suggesting this sample dataset is appropriate for further evaluation.

At Aeropuerto (~26.5 km NE of Inglés; Fig. 1C), the distribution of winds was N unimodal with a $\overline{\theta}$ of 6° and $\overline{U}$ of 8.3 m s^{-1}, recording similar conditions to the longer term wind data collected at this site (i.e., Fig. 1B). At El Matorral (~7 km NE of Inglés; Fig. 1C), unimodal winds shift towards the NNE ($\overline{\theta} = 22°$) and $\overline{U}$ is reduced to 5.8 m s^{-1}. At Inglés (~ 3.5 km SE of Maspalomas; Fig. 1C), the winds shift towards the NE ($\overline{\theta} = 55°$) and $\overline{U}$ is further reduced to 5.2 m s^{-1}. Here, a noticeable bimodality of airflow develops with a distinct westerly component not recorded at the previous two stations. At Maspalomas (Fig. 1C), this observed bimodality increases with a strong SW wind component, although $\overline{\theta}$ remains NNE at 15° and $\overline{U}$ is reduced to 3 m s^{-1}. Despite all stations being located on a ~ 32 km-long section of low-lying relief in

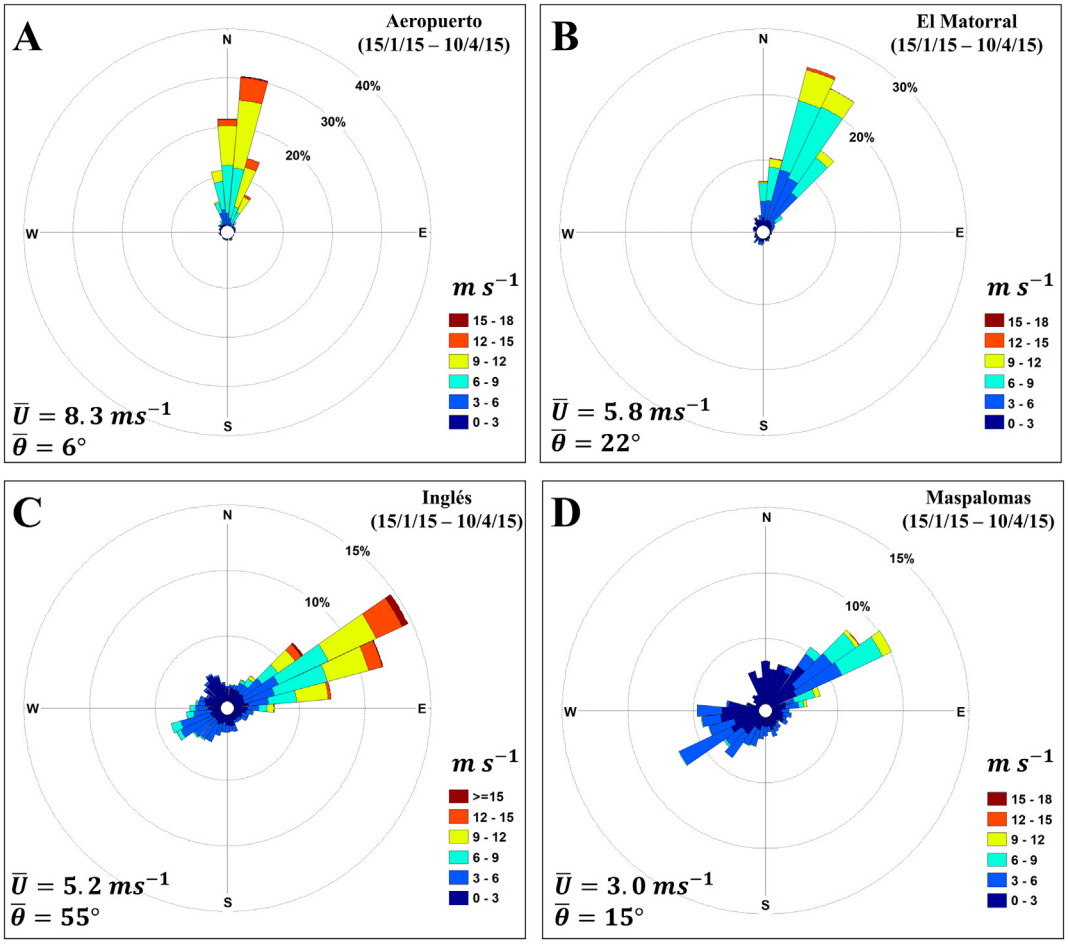

Fig. 2. Hourly wind data between January and April 2015 for Aeropuerto (A), El Matorral (B), Inglés (C), and Maspalomas (D). Data are averaged over this three-month time period for wind velocity ($\overline{U}$) and directionality ($\overline{\theta}$) for each sample site.

the eastern-southern section of the island, considerable inter-site variability exists between the datasets recorded over the three-month sample period.

4.2. Meso-scale LES simulations

4.2.1. Case 1: NNE winds

Case 1 simulated airflow from the NNE, the primary directional component of the regional wind regime taken from the most consistently recording meteorological station (i.e., Aeropuerto; Fig. 1B). Model results display unperturbed wind directions at Aeropuerto and El Matorral, maintaining a NNE orientation (Fig. 3A,B). These sites did display an acceleration of flow velocity with overall increase in U_δ of over 57% at Aeropuerto and 65% at El Matorral, compared to the model inlet (Table 1A). Flow deflection or θ_Δ was recorded at Inglés and Maspalomas, where winds recorded a consistent NE orientation (Fig. 3C,D). At Inglés, U_δ was 17% higher than at the model inlet, whereas Maspalomas recorded a decrease in U_δ of −17% (Table 1A). Wind conditions remained largely consistent at each sample sight with little fluctuation during the 24-h model simulation with maximum *TI* values of ≤ 0.01, $U_\sigma \leq 0.05$ m s^{-1}, C_I of 99, and θ_σ of ≤ 0.46° for each sample site (Table 1A). Despite this intra-site consistency, unique patterns of flow acceleration, deceleration, and deflection were observed between sites during Case 1.

4.2.2. Case 2: north winds

During simulated N airflow conditions for Case 2, Aeropuerto and El Matorral display a consistent $\overline{\theta}$ from the N and NNE, respectively (Fig. 4A,B). Inglés and Maspalomas also record $\overline{\theta}$ from the N; however, these sites display a high variability in the daily range of directional orientations (Fig. 4C,D). At these sites, instantaneous θ primarily fluctuated between the W and E directions (Fig. 4C,D), with up to 180° divergence of between sites recorded simultaneously. All sample sites display a decrease in time-averaged U_δ with the highest reduction occurring at Inglés (Table 1B). While Aeropuerto and El Matorral display highly consistent $\overline{U}$ with $U_\sigma < 0.6$ m s^{-1}, Inglés and Maspalomas display considerable gustiness with instantaneous *U* fluctuating widely between >0 to >5 m s^{-1} (Fig. 4C,D). Increased U_σ, θ_σ, and *TI* at Inglés and Maspalomas indicate highly turbulent conditions near the Maspalomas dunefield, developing during N winds.

To isolate directional and velocity fluctuations at Inglés and Maspalomas, the Savitzky-Golay filter was used to reduce the noise of the instantaneous data while maintaining spectral peaks that represent the upper limits of fluctuations away from the mean (Savitzky and Golay, 1964). This smoothing technique has previously been applied to identify turbulent fluctuations in meteorological data (e.g., see Parton et al., 2010). During Case 2, Inglés displays characteristic spectral peaks of 42° away from its mean every ~2 h (Fig. 5A). Maspalomas displays smaller scale variability with fluctuations of 21° away from its mean occurring every ~1.5 h (Fig. 5A). The root mean square difference (RMSD) records an average of 34° of variation in θ between Inglés and Maspalomas over the 24-h sample period. Velocity variability was also identified at Inglés displaying a ~ 1 m s^{-1} fluctuation around its mean every ~2.3 h (Fig. 5B), whereas Maspalomas recorded a variation in velocity of ~1 m s^{-1} every ~1.6 h (Fig. 5B). On average, the RMSD between the two sites records a variability of ~0.7 m s^{-1}. The consistency of the fluctuating directional and velocity values, ranging from below to

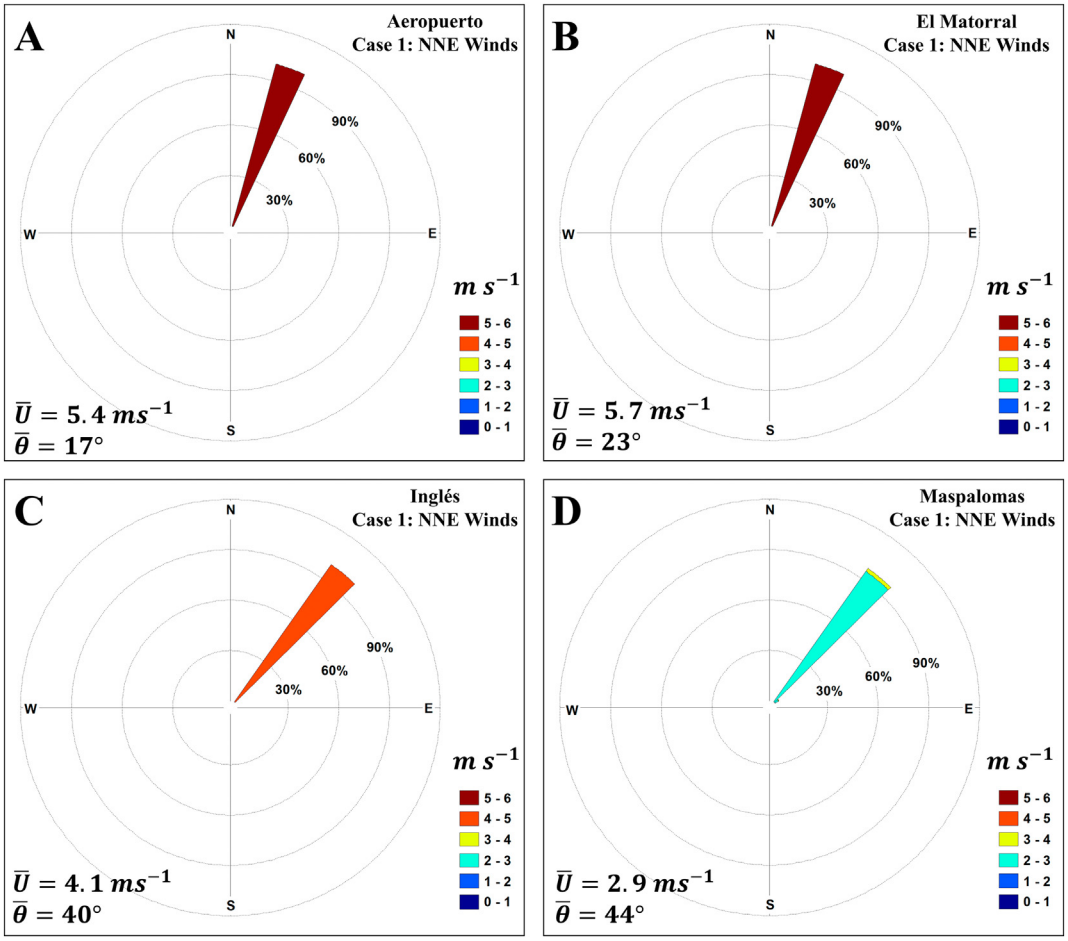

Fig. 3. Wind data during NNE simulations for Aeropuerto (A), El Matorral (B), Inglés (C), and Maspalomas (D). Data are averaged over a 24-h period for wind velocity $\overline{U}$ and the direction $\overline{\theta}$ for each sample site.

above threshold conditions, suggest that coherent turbulent flow structures at these sample sites are capable of modifying sediment transport gradients within the dunefield.

4.2.3. Case 3: NNW winds

Case 3 simulated NNW wind conditions and displayed significant steering between the sample sites. At Aeropuerto, θ_Δ was deflected 11% to a consistent NNE direction and a reduction of U_δ was recorded by over 50% (Fig. 6A; Table 1C). Note that during incremental changes to the incident flow direction for all three cases (i.e., 1–3), Aeropuerto repeatedly records a narrow 8° arc between N-NNE winds. El Matorral showed highly variable instantaneous wind conditions with U_σ of 0.87 m s^{-1} and θ_σ of over 49°. At both Inglés and Maspalomas θ_Δ is deflected towards the west, maintaining a largely NW orientation at each site (Fig. 6C,D; Table 1C). Inglés experiences a reduction in U_δ of −22% whereas Maspalomas records a slight increase in U_δ of 4% (Table 1C). El Matorral, located in the lee of the island during Case 3, displays the largest variation of flow velocity and directionality, highest *TI* of 0.5, and lowest C_I of 63.

Table 1
Wind perturbations for Aeropuerto (1), El Matorral (2), Inglés (3), and Maspalomas (4) recorded over a 24-h model simulation during Case 1 (NNE), Case 2 (N), and Case 3 (NNW) winds. Recorded wind conditions include, the speed-up perturbation ratio (U_δ%), turbulence intensity (*TI*), velocity standard deviation (U_σm s^{-1}), directional perturbation ratio (θ_Δ%), consistency index (C_I), and direction standard deviation for each site (θ_σ°; i.e., 1–4).

Source	Site	U_δ %	U_σ m s^{-1}	θ_Δ %	θ_σ °	C_I	*TI*
A. Case 1: NNE Winds	A. Aeropuerto	57	0.00	−2	0.01	99	<0.01
	B. El Matorral	65	0.00	0	0.01	99	<0.01
	C. Inglés	17	0.02	5	0.12	99	<0.01
	D. Maspalomas	−17	0.05	6	0.46	99	0.01
B. Case 2: N Winds	A. Aeropuerto	−10	0.01	2	0.16	99	<0.01
	B. El Matorral	−26	0.06	5	0.88	99	0.02
	C. Inglés	−38	1.05	3	41.58	73	0.46
	D. Maspalomas	−8	1.18	−1	28.04	88	0.33
C. Case 3: NNW Winds	A. Aeropuerto	−57	0.03	11	0.74	99	0.01
	B. El Matorral	−53	0.87	1	49.06	63	0.5
	C. Inglés	−22	0.92	−1	13.01	97	0.23
	D. Maspalomas	4	0.84	−3	10.1	98	0.17

4.3. Meso-scale topographic controls

Meso-scale topographic steering (e.g., VKVS) can often become visible in the stratocumulus cloud layer that forms below a temperature inversion layer (i.e., ~400–1000 m for Gran Canaria; Naya, 1984; Barton et al., 2000) around mountainous island chains (Conover, 1964; Zimmerman, 1969; Jensen and Agee, 1978; Etling, 1989). Here horizontal flow dominates as vertical flow over island topography is suppressed (Zimmerman, 1969; Etling, 1989), typically due to the presence of a capping inversion in the atmospheric boundary layer. Our results report airflow at 50 m above the model surface, well below a potential inversion layer around the island perimeter. It must be noted that the current S-LES simulation approach cannot cover all the atmospheric boundary layer characteristics of a capping inversion but aimed to mimic its vortex shedding characteristics with a more typical unstable boundary layer profile. It would be important to pursue more complete modelling practices that may duplicate the thermal boundary layer character as

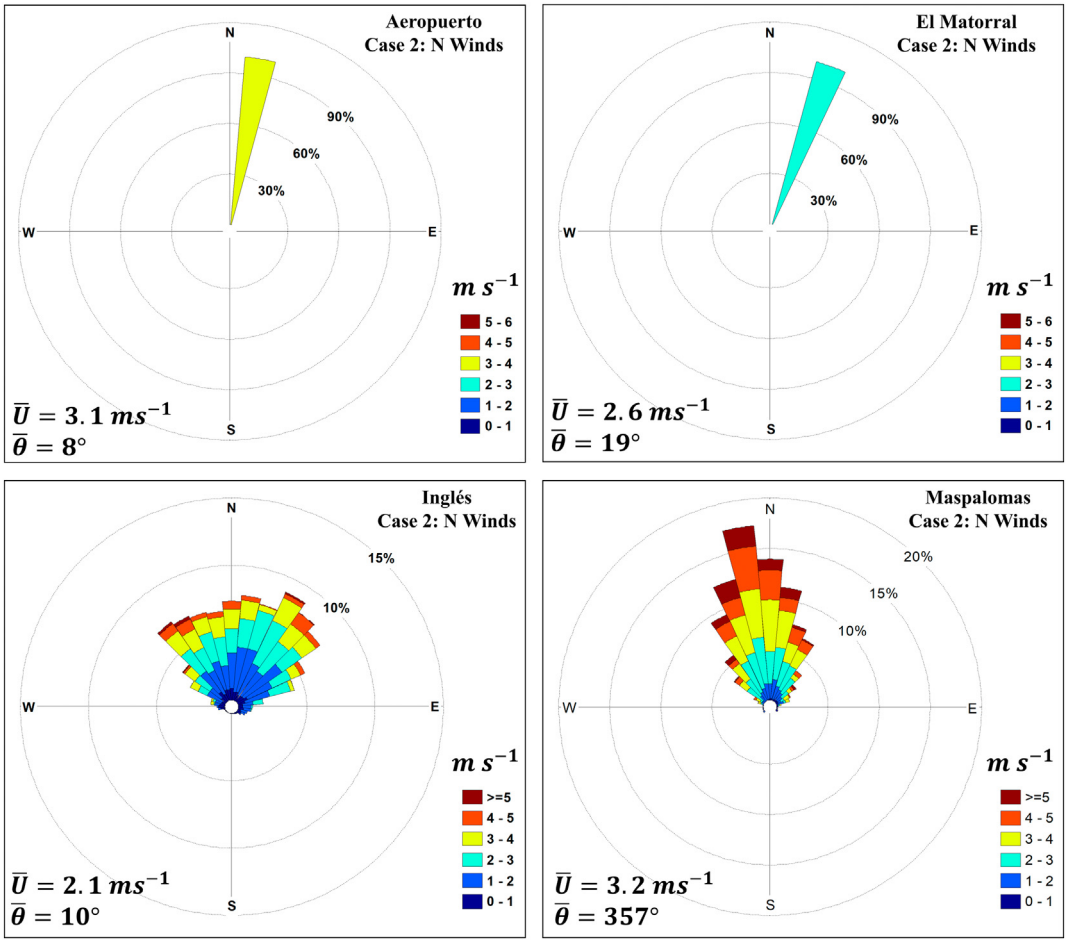

Fig. 4. Wind data during N simulations for Aeropuerto (A), El Matorral (B), Inglés (C), and Maspalomas (D). Data are averaged over a 24-h period for wind velocity $\overline{U}$ and the direction $\overline{\theta}$ for each sample site.

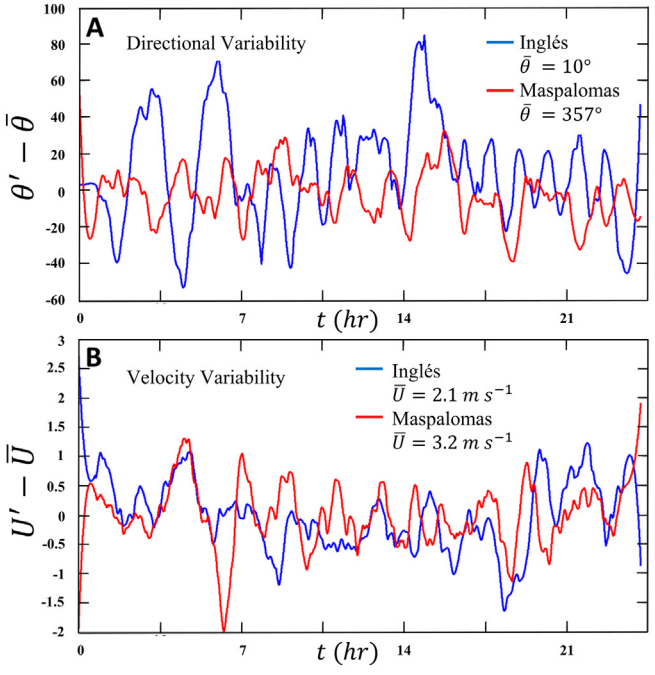

Fig. 5. Filtered instantaneous directional (A) and velocity (B) values, deviating from the mean, for Inglés and Maspalomas showing characteristic fluctuations in airflow conditions over the 24-h model simulation.

well, as it may intensify the modelled vortex shedding phenomena, but is beyond the scope of this current work.

CFD model simulations show meso-scale (10s km) bifurcation of near-surface airflow occuring around the island. Island-scale topographic steering is aided by pressure differentials as airflow approaches to, is deflected around, and passes by the island topography (Jensen and Agee, 1978). The varying pressure gradients developing around the island are visible from our model results (Fig. 7A). During N winds, airflow is compressed and an adverse pressure gradient develops on northern side of the island (Fig. 7A), leading to the stagnation of airflow and a reduction of velocity. A negative pressure gradient then forms around the western and eastern coasts, promoting airflow to accelerate and move parallel to the lateral coastlines (Figs. 7A,B). In the lee, an unstable adverse pressure gradient develops as airflow converges at the lee side coast promoting an increase in turbulent conditions and eddy shearing downwind of the island (Figs. 7A,B). Flow bifurcation represents a dominate topographically steered airflow process at the whole-island scale that develops primarily in lower altitude coastal areas that are below the inversion layer.

The complexity of localized topography around Gran Canaria also contributes to smaller meso-scale steering (i.e., ~2 km), observed at Inglés and Maspalomas (Case 2; Fig. 7D). Canyons extend down from the island interior towards the coast leading to further topographic steering, or canyon breezes, that modifies the approaching airflow direction and velocity, particularly in unstable lee side zones (e.g., Figs. 4C,D; 6B). This is visible at the Maspalomas dunefield during N wind conditions (Fig. 7D), where approaching flow can become deflected and constrained by the upwind canyon topography before expansion takes place across the Maspalomas

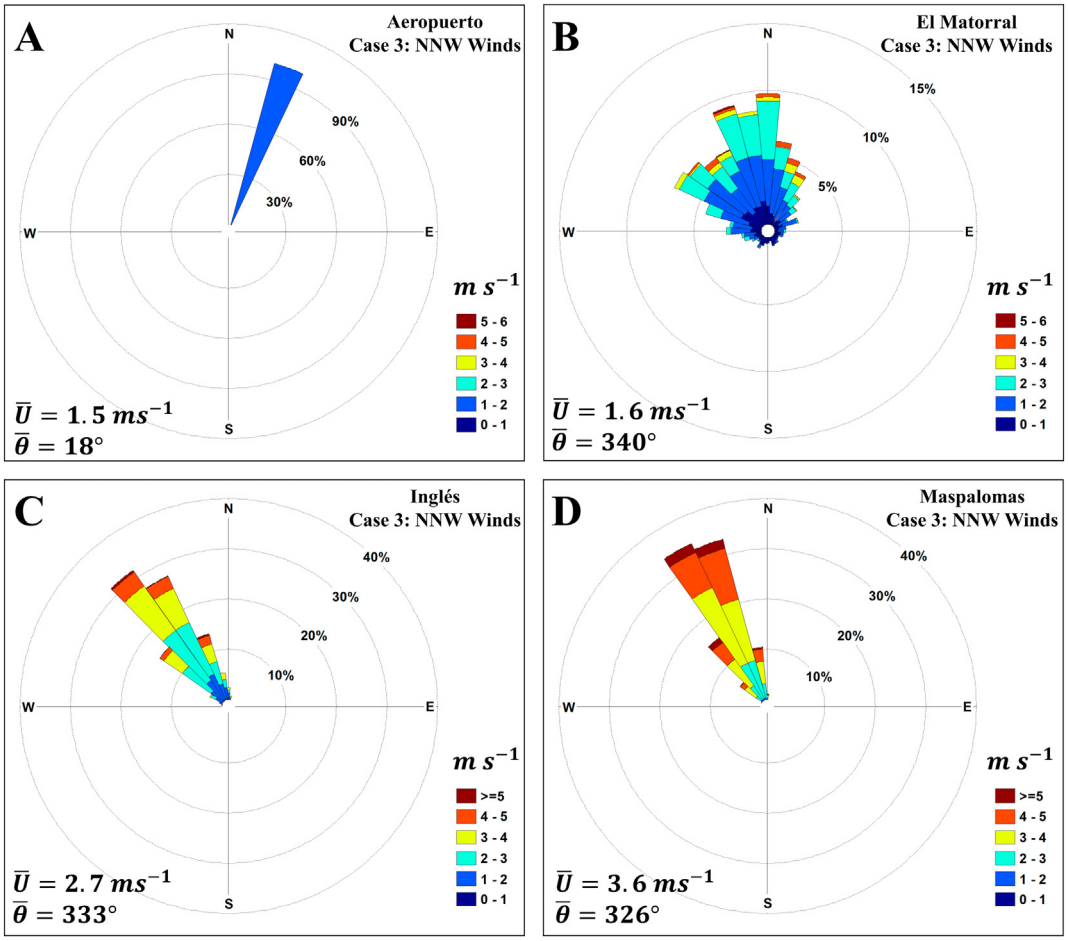

Fig. 6. Wind data during NNW simulations for Aeropuerto (A), El Matorral (B), Inglés (C), and Maspalomas (D). Data are averaged over a 24-h period for wind velocity $\overline{U}$ and the direction $\overline{\theta}$ for each sample site.

dunefield. This contributes to the production of turbulence, producing gusty winds with diverging and converging flow directions between the eastern (i.e., Inglés) and western (i.e., Maspalomas) sections of the dunefield (Figs. 4C,D; 5A,B). Northerly wind conditions predominate at Gran Canaria; however, slight changes in the incident angle of flow can significantly alter flow at the Maspalomas dunefield from perturbed uni-directional NE (i.e., Case 1), perturbed uni-directional NNW (i.e., Case 3), and perturbed multi-directional N (i.e., Case 2) flow conditions.

4.4. Dune dynamics

4.4.1. Global wind retro-analysis and sand drift potential

Airflow conditions, predicted for the upwind oceanic surface winds by the MERRA-2 retro-analysis model, show similar wind patterns between t_1 and t_2 (Table 2A). Both time series display unimodal winds with a slight northerly shift in $\overline{\theta}$ from 27° (NE) during t_1, to 15° (NNE) during t_2 (Table 2A). Both time series recorded average velocities above threshold conditions (i.e., taken as ≥5.5 m s^{-1}) with $\overline{U}$ of ~6 m s^{-1}, although a noticeable increase in the percentage of days per year above threshold ($>u_{*t}$ %) occurs between t_1 (57%) and t_2 (64%; Table 2A). Divergent wind events (DWEs; i.e., defined as days with above threshold conditions and $-20\% < \overline{\theta}_{\Delta} > 20\%$), occurring between the E – NW, only showed a small increase between t_1 and t_2 accounting for 4% and 5% of the total days $>u_{*t}$, respectively. The last DWEs occurred over a one day-period more than 3 months prior to the end of t_1 ($\overline{U}$ = 6.53 m s^{-1} and $\overline{\theta}$ = 239°) and over a two-day period more than 4 months prior to the end of t_2 ($\overline{U}$ = 7.84 m s^{-1} and $\overline{\theta}$ = 284°). NNW-ENE events with similar or higher magnitudes occurred for the remainder of these time periods and represent over 95% of all days with above threshold conditions.

Higher magnitude velocities and more days above threshold were recorded during t_2, resulting in a relatively large increase in drift potential (DP) but not resultant drift potential (RDP) during this period (Table 2B). The directional drift potential (DDP) shifts slightly from t_1 (206°) to t_2 (198°) in response to the higher percentage of N winds (Table 2A,B); however, both time periods maintain a predicted drift towards the SSW direction. Despite this consistency in DDP, the RDP/DP ratio indicates that the variability of competent winds increases, ranging between narrow unimodal in t_1 (0.92) to wide unimodal in t_2 (0.81; Table 2B). This increase in variability is in response to the higher magnitude of $\overline{U}$ during DWEs accounting for 10% of total DP, compared to 5% of total DP in t_1. Despite the influence of DWEs on predicted DP, at least 90% of DP values were recorded between the NNW-ENE for both time periods. Given the predicted airflow conditions and sand drift potentials, competent winds from the NNW-ENE are identified as the dominate regional wind regime during both t_1 and t_2.

4.4.2. Crest migration and mass flux analysis

Analysis of dune migration patterns consisted of the crest displacement and direction measurements from a total of 687 samples for t_1 and 445 samples for t_2. Given rapid migration rates and less pronounced topographic breaks at the crest, the small barchan dunes located in the eastern section of the dunefield were excluded from this study as the

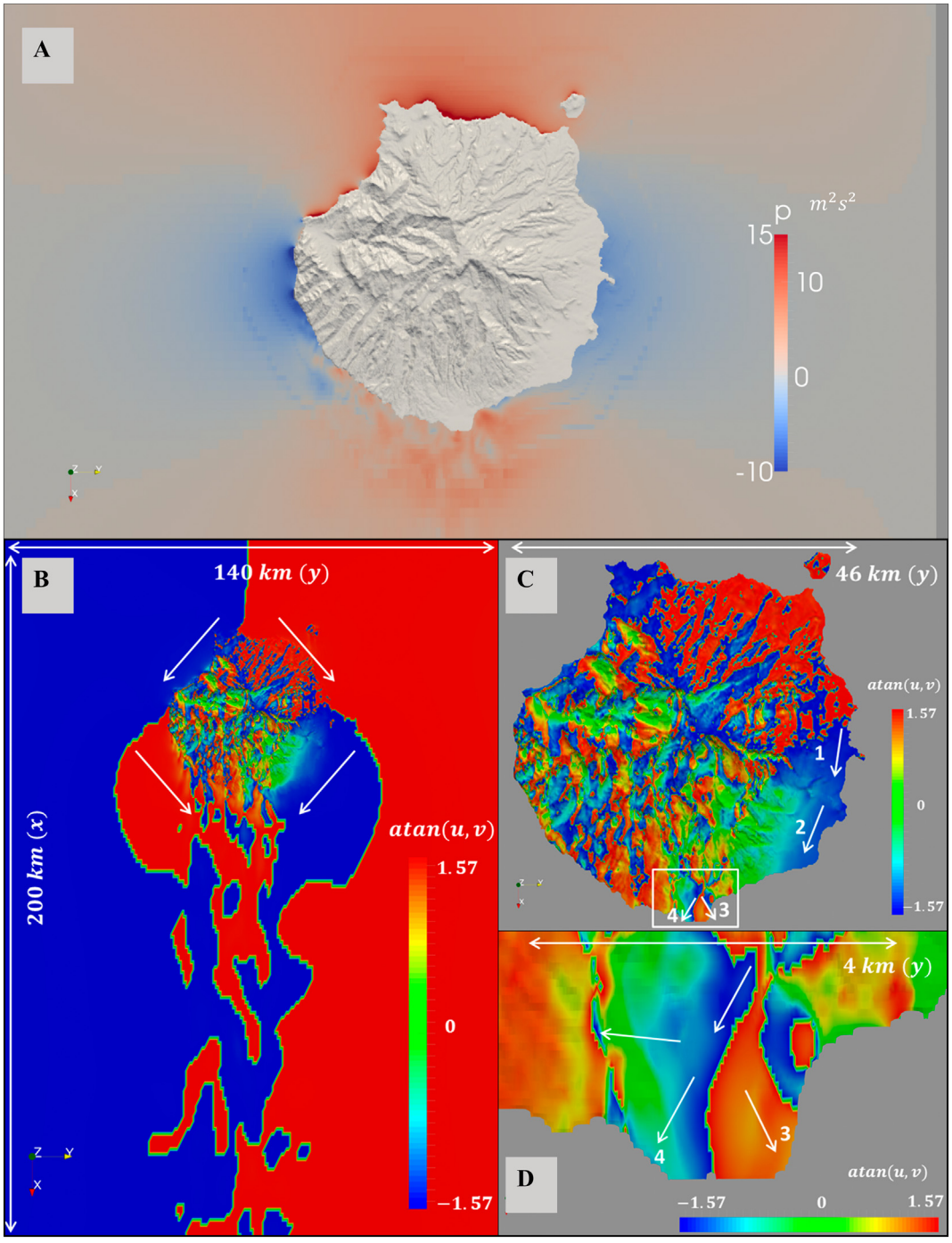

Fig. 7. Pressure gradients developing around Gran Canaria, promoting meso-scale airflow steering (A). Island-scale bifurcation of airflow around Gran Canaria and vortices developing downwind of the island topography (B). Low relief coastal areas on the lateral coasts are controlled primarily by their location relative to steering of airflow around the island (C). In the lee (i.e., sites 3 and 4), airflow is additionally modified by the upwind canyon topography causing turbulent conditions across the Maspalomas dunefield.

current methods are not suitable for monitoring their migration through time. This likely provides a conservative estimation of average celerity rates ($\bar{c}$) as dunes in these locations have been recorded to migrate up to 34 m y^{-1} (Hernández et al., 2007; Pérez-Chacón Espino et al., 2007; Jackson et al., 2013b). Therefore, results report crest celerity (c) and celerity direction (θ_c) for the barchanoid dune ridges in the central section, and the discrete barchan dunes located in the southwest section of the dunefield.

Although both regional wind velocities and sand drift potentials increased during the second time series (Table 2A,B), $\bar{c}$ reduced significantly from 7.26 m y^{-1} in t_1, to 2.80 m y^{-1} in t_2 (Table 2C). Standard deviations of celerity (c_σ) and celerity directions ($\theta_{c\sigma}$) increased and the confidence index (C_I) decreased in t_2 (Table 2C), highlighting a shift from highly uniform to variable dune dynamics observed between the time periods. During t_1, 90% of dunes migrated towards the WNW-SSW. In comparison, only 62% of dunes migrated in these directions in t_2 and 28% of dune crests were reversed or migrated towards the NNE-SSE. Crest reversals up to 180° in opposition of the $\overline{U}$ (Table 2A) and DDP (Table 2B) were recorded, displaying a significant divergence between the regional wind and observed dune dynamics during t_2.

Table 2
(A.) Predicted up wind oceanic wind conditions from the MERRA-2 retro-analysis model between 2006 and 2011, occurring between time series 1 (t_1) and time series two (t_2) including average velocity ($\overline{U}$ m s^{-1}) and standard deviation (U_σ m s^{-1}), average direction ($\overline{\theta}$ °) and standard deviation (θ_σ°), consistency index (C_I), and percentage of days per year exceeding the transport threshold ($>u_{*t}$ %). (B.) Predicted wind conditions analyzed by the 'Fryberger Model' (FM), including drift potential (DP), resultant drift potential (RDP), directional drift potential (DDP), and the ratio between RDP/DP. (C.) Dune migration patterns observed from LiDAR DEMs between t_1 and t_2, including average crest celerity per year ($\overline{c}$ m y^{-1}) and standard deviation (c_σ m y^{-1}), average direction of crest celerity ($\overline{\theta_c}$ °) and standard deviation ($\theta_{c\sigma}$°), consistency index (C_I), and percentage of crest reversals observed (reversals %). (D.) Mass Flux (MF) analysis including the average mass flux ($\overline{MF}$ mt m y^{-1}), average resultant mass flux ($\overline{RMF}$ mt m y^{-1}), average direction of mass flux ($\overline{DMF}$ °), and the ratio between $\overline{RMF/MF}$.

Source	Metric	Time Series 1 (t_1) 2006–2008	Time Series 2 (t_2) 2008–2011
A. Merra-2 Global Wind Retro-Analysis: 2006–2011	$\overline{U}$ m s^{-1}	5.98	6.26
	U_σ m s^{-1}	2.14	2.20
	$\overline{\theta}$ °	27	15
	θ_σ°	46	45
	C_I	71	72
	$>u_{*t}$ %	57	64
B. Fryberger Model (FM)	DP	73	86
	RDP	67	70
	DDP °	206	198
	RDP/DP	0.92	0.81
C. LiDAR DEMs: 2006, 2008, and 2011	$\overline{c}$ m y^{-1}	7.26	2.80
	c_σ m y^{-1}	4.03	6.64
	$\overline{\theta_c}$ °	250	248
	$\theta_{c\sigma}$°	34	82
	C_I	83	35
	Reversals %	1	28
D. Mass Flux (MF) Analysis	$\overline{MF}$ mt m y^{-1}	113	36
	$\overline{RMF}$ mt m y^{-1}	107	27
	$\overline{DMF}$ °	248	236
	$\overline{RMF/MF}$	0.94	0.76

The observed decrease in c between t_1 and t_2 resulted in a significant reduction in the average mass flux ($\overline{MF}$ mt m y^{-1}) and average resultant mass flux ($\overline{RMF}$ mt m y^{-1}) predicted across the 1.22 km^2 dunefield observation area (Table 2D; Fig. 8). *MF* values show considerable heterogeneity between time series with the majority of the dune surfaces highly active in t_1, apart from the deflationary areas at the eastern and western extents (Fig. 8). In contrast, only the taller barchanoid dune ridges to the east and south of the urban terrace remain moderately active in t_2. The average direction of mass flux ($\overline{DMF}$ °) only shifted slightly southward during t_2, although high variability of flux directions can be observed in the western section of the dunefield during t_2 (Fig. 8). Here, flux directions range largely between SSW-ESE, whereas the barchanoid dune ridges to the east maintain a consistent westerly flux direction. This variability corresponded to a decrease in $\overline{RMF/MF}$ between t_1 which was narrow unimodal (0.94; Table 2D; Fig. 8), to t_2 where flux directions can be classified as acute bimodal (0.76; Table 2D; Fig. 8).

Comparing the predicted sand drift potential (DP) and the mass flux (MF) observed within the dunefield show inconsistent relationships between the two time-series. DP values, converted into mass flux using the methods described in (Fryberger and Dean, 1979) and Eq. (17), predicts a mass flux of ~86 mt m y^{-1} for t_1 and ~ 103 mt m y^{-1} in t_2. This corresponds to flux values that were underestimated by 23% and overestimated by 186% during each respective time series, relative to MF estimates. The disparity between the two metrics is particularly evident for t_2. In part this may be influenced by a reduction in sediment supply (i.e., decrease in dune elevations and increase in deflationary areas) and erodibility (i.e., increase in vegetation in the urban shadow zone) that are not accounted for in the FM; however, the lower rates of *MF* observed across the entire dunefield cannot be readily explained by the corresponding regional airflow that predicted increased erosivity during this time period (Table 2A,B). Furthermore, DDP values predicted unimodal sand drift towards the SSW for both time periods, differing from the observed unimodal sand flux towards WSW in t_1 and bimodal sand flux towards the S and WSW in t_2.

5. Discussion

By analysing the inconsistencies in the available meteorological station data (Fig. 2), CFD model results (Section 4.1), regional wind retro-analysis (Section 4.2.1), and dune dynamics (Section 4.2.2), evidence suggests that significant topographic steering of the regional airflow patterns occurs around the coast of Gran Canaria. Meso-scale airflow perturbations, both observed (Fig. 2) and modelled (Figs. 3, 4, 5, 6, 7; Table 1), result in a complex regional wind regime that are site-dependent relative to the incident angle of airflow and adjacent topography (Fig. 8). Despite consistent airflow conditions predicted between t_1 and t_2 (Table 2A), dune migration, drift direction, and mass flux show diverging patterns of sediment mobility between periods (Fig. 8). Distinct signatures of bimodal wind conditions (e.g., crest deflections and reversals), developing during t_2, cannot be accounted for in the available regional airflow records or through global wind retro-analysis models. This evidence suggests that local airflow patterns are modified by meso-scale topographic steering and, as a result, could affect the divergent dune dynamics observed at Maspalomas.

5.1. Interpreting the regional wind regime

During all of our model simulations (Cases 1–3), each site experienced varying magnitudes of flow acceleration or deceleration, flow deflection, and turbulence (Table 1). The level of divergence from upwind conditions is primarily controlled by: (1) The incident wind direction relative to island-scale bifurcation (i.e., located on the lateral coast or on the unstable lee-side), and (2) The topographic relief adjacent to the sample site. For instance, during all S-LES simulations Aeropuerto displays consistent N-NNE winds within an 8° arc for each incident wind direction (i.e., NNE, N, and NNW). This is a result of both Aeropuerto's position on the eastern coast of the island where airflow is steered parallel along the coastline and low topographic relief that does not further modify approaching flow conditions. This indicates that using wind data from Aeropuerto, the longest and most continuous record of airflow on Gran Canaria, to characterize the regional wind regime for other sites on the southeastern coastline could include significant directional and magnitude bias. For example, during NNE wind simulations (i.e., Case 1) an easterly shift and relative deceleration of winds were observed at Inglés and Maspalomas, consistent with previous observations at the dunefield (Nadal and Guitián, 1983; Martínez et al., 1986; Martínez, 1990; Naranjo, 1999; Hernández-Calvento, 2006; Viera-Pérez, 2015).

Sites at Inglés and Maspalomas, recorded highly variable wind directionality, velocity, and turbulence during N wind conditions (Case 2; Table 1B) because of their location in the lee of the island and high-profile upwind canyon terrain. Airflow bifurcation around the island converges at this location leading to flow deceleration and unstable conditions that fluctuate between easterly and westerly wind components. Additionally, turbulent canyon breezes contribute to highly variable instantaneous wind directions diverging up to 180° between sites and gusts that exceeded the daily velocity averages by up to 47%, corresponding to simultaneous and daily observations of opposing wind patterns within the dunefield (Hernández-Calvento, 2006; Máyer-Suárez et al., 2012). As a result, coherent turbulent flow structures developing over a period of 1–2 h could produce non-uniform sediment transport gradients within the dunefield, not apparent from longer duration averages (Table 1B) or upwind meteorological wind references (e.g., Aeropuerto; Fig. 4A).

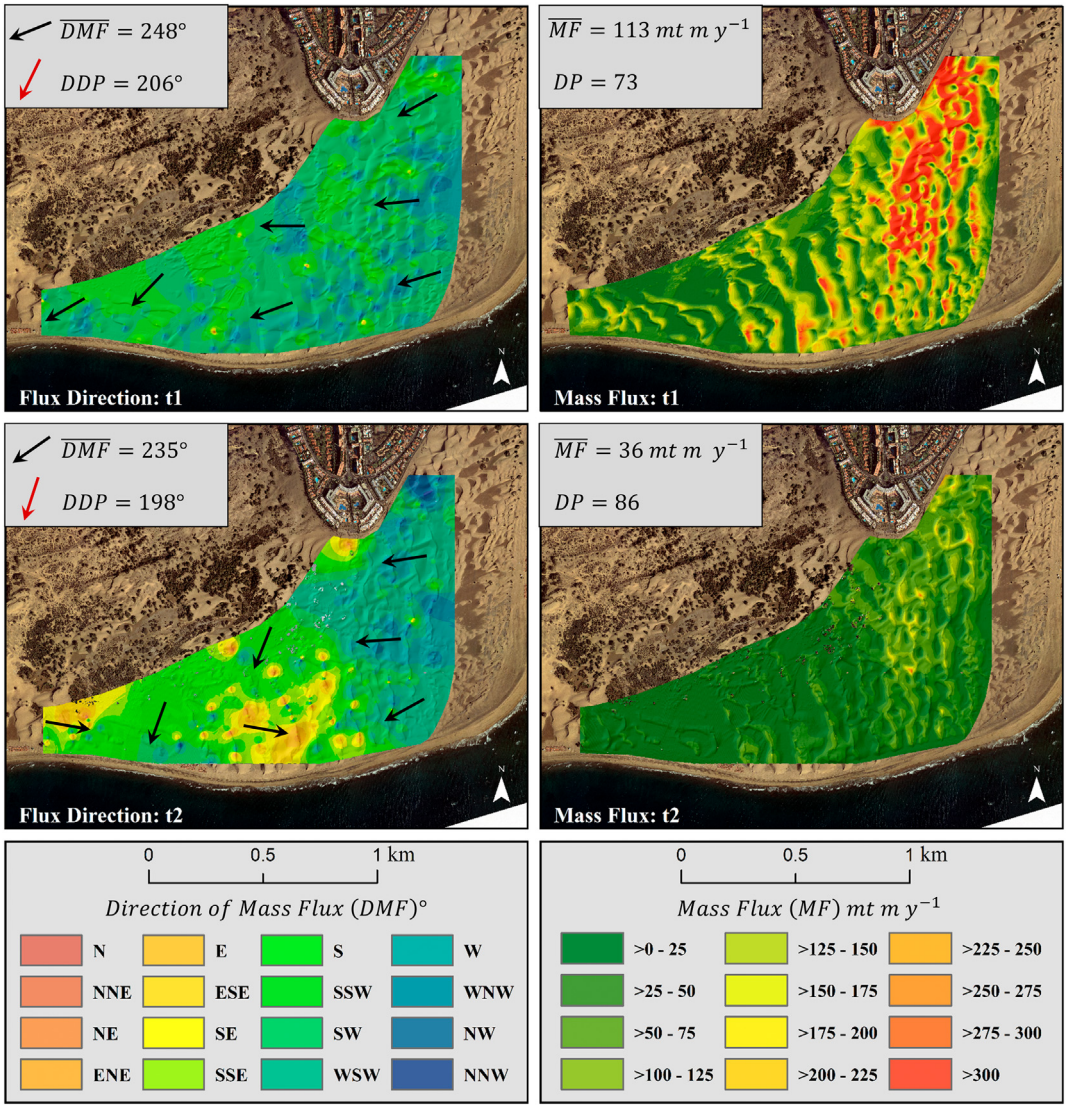

Fig. 8. Direction of mass flux (DMF °) and mass flux (MF mt m y^{-1}) observed between time series 1 (t_1) and time series 2 (t_2) across 1.22 km^2 of dunes at Maspalomas. Additionally, the average mass flux direction ($\overline{DMF}$ °), average mass flux ($\overline{MF}$ mt m y^{-1}), and directional drift potential (DDP) and drift potential (DP) predicted by the Fryberger Model (FM) are included in the map insets.

During NNW conditions (Case 3), Inglés and Maspalomas experienced a westerly shift in average wind directions from the NW. As the upwind incident angle deviates westerly from N, these sites may experience additional deflection westward as winds bifurcate around the island. Further evidence from the simultaneous meteorological wind records (Fig. 2) show a distinct bimodality of winds at Inglés and Maspalomas from the SW-NE, whereas Aeropuerto and El Matorral display unimodal winds primarily from the NNW-NE. Simulated daily velocity averages, relative to unperturbed upwind flow, increased at Maspalomas by 4% and decreased at Inglés by −22% (Table 1C). This suggests that during westerly winds, the western section of the dunefield could experience a relative increase in erosivity, consistent with modifications to dune landforms in this area (Smith et al., 2017a) and observations of topographic steering around the western coastline (Viera-Pérez, 2015). Evidence from previous studies, meteorological records, and CFD model results indicate the significant topographic airflow steering around Gran Canaria, capable of modifying local aeolian processes at Maspalomas.

5.2. Interpreting dune dynamics

Barchan dunes develop primarily in arid environments with low vegetation cover, low sediment supply, and unimodal wind conditions (Bagnold, 1941; Fryberger and Dean, 1979; Wasson and Hyde, 1983). Tsoar (1985) suggests that barchan dunes reach a steady state under unidirectional winds characterized by a convex profile caused by a progressive increase in erosive potential up the stoss slope. In contrast, bimodality of wind conditions can cause a variety of barchan dune asymmetries including temporary slip faces developing on the stoss slope, irregular lateral arm extension, and dune collision (Bagnold, 1941; Bourke and Goudie, 2009; Bourke, 2010; Parteli et al., 2014). Elbelrhiti and Douady (2011) found that even under largely unidirectional winds in the Moroccan Atlantic Sahara, barchan dunes are in a constant state of disequilibrium in response to slight variability in incident wind conditions. Signatures of these modified dune forms can last between hours to over a year depending on the wind strength and size of the barchan dunes (Elbelrhiti and Douady, 2011; Elbelrhiti, 2015).

Evidence of a variable wind regime including barchan dune asymmetry, crest deflections and reversals, and lower migration and flux rates can be identified across the western section of the dunefield. This was particularly evident in our second time series (t_2), where sediment transport patterns varied considerably within the dunefield and relative to highly uniform conditions observed in t_1 (Fig. 8). Results of the Merra-2 retro-analysis recorded consistent unimodal NNE winds accounting for over 95% of days exceeding the sediment transport

threshold for both time series. The magnitude of divergent wind events (DWEs) did increase during t_2, but only accounted for 10% of the predicted sand drift potential (DP). The last DWE occurred four months prior to the LiDAR survey in 2011, with similar or higher magnitude events recorded from the dominant NNW-ENE regime for the remainder of the time series. Additionally, high magnitude DWEs (i.e., from the SW) are often associated with heavy rainfall, further limiting aeolian transport during these time periods (Máyer-Suárez et al., 2012). This suggests that it is unlikely that observed dune dynamics following t_2 are a result of temporary adjustments to DWEs but represent a more consistent modification to localized aeolian dynamics within the dunefield.

Comparisons between regional wind records, potential sand drifts, and dune dynamics reveal clear inconsistencies at Maspalomas. A reliance on regional meteorological station or retro-analysis data can lead to over- or under-estimation of the processes responsible for localized sediment mobilization. Given the lack of consistent meteorological station data from Inglés and Maspalomas or in-situ measurements covering the period between surveys, this study relies on the observed dune dynamics as an indicator of a more complex wind regime operating at this site. This manifests in the variability of dune migration rates, morphometry, and sediment transport pathways through time (Table 2C, D; Fig. 8). This disparity, unaccounted for in regional airflow retro-analysis (Table 2A,B) or the longer-term regional meteorological reference (Fig. 1B), provides further evidence that meso-scale topographic steering around Gran Canaria can modify localized wind conditions responsible for variable dune dynamics at Maspalomas.

5.3. Multi-scale considerations and future research

Previous meso-scale models for Gran Canaria have simulated airflow steering around the coastline (i.e., developed by the ITC) and the influence of urban development on flow acceleration or deceleration at Maspalomas (Hernández-Calvento et al., 2014). CFD models can be used to improve simulations of flow, particularly turbulent fluctuations (Smyth, 2016), including analysis of the instantaneous three-dimensional flow vectors and characterization of coherent turbulent flow structures presented in Section 4.2. Previous CFD studies at Maspalomas have also identified turbulent flow patterns and predictions of the sediment flux potential derived from the wall shear stress at the model surface, around the urban area (Smith et al., 2017b) and over bachan dune and interdune topography (Smith et al., 2017a). At larger scales, this study was able to simulate two additional sources of turbulent airflow perturbations, including flow convergence at the unstable lee-side coastline and canyon breezes that can additionally modify approaching flow. Cumulatively, these models indicate a unique environment where erosivity within the dunefield is being modified by topographically and anthropogenically steered airflow at multiple scales, providing new context for observed dune dynamics at this site.

Scaling our understanding of aeolian processes, from micro-scale sediment flux formulas to regional wind regimes and remotely sensed dunefield patterns, has previously been proposed by Fryberger and Dean (1979). The simplicity of the 'Fryberger Model' (FM) has made it a widely used descriptor of the competent wind conditions in aeolian environments; however, attempts to compare a FM approach to actual field data can often lead to significant inconsistencies in both the magnitude and direction in which sediment is being mobilized (e.g., Smith et al., 2017c). The limitations of the original FM have been well documented and may include: (1) Errors with unit conversions (Bullard, 1997), (2) A magnitude and frequency bias that are a result of binning data into standard velocity and directional classes (Pearce and Walker, 2005), and (3) Lack of consideration of transport limiting conditions (e.g., surface moisture, fetch length, snow cover, etc.; (Nickling and Davidson-Arnott, 1990; Bauer and Davidson-Arnott, 2003; Delgado-Fernandez, 2010; Delgado-Fernandez and Davidson-Arnott, 2011; Delgado-Fernandez et al., 2012, 2013b).

An essential assumption of the FM is an erodible bed with bedforms no larger than ripples (i.e., regional winds are unperturbed), so it is unsurprising that DP estimates deviate from dunefield observations at Maspalomas. This disparity may be more become more evident in anthropogenically modified systems (Nordstrom and McCluskey, 1984; Hernández-Calvento et al., 2014; Smith et al., 2017a) or in areas surrounded by high profile topography (Wiggs et al., 2002). Local scale processes are further modified in all dune environments in response to surface roughness elements (Arens, 1996; Hesp et al., 2005) and coastal (Lynch et al., 2010; Bauer et al., 2012) and desert dune morphometry (Walker, 1999; Baddock et al., 2011), thereby modifying localized sediment transport gradients. In the absence of long-term field measurements and consideration for site specific contingencies (e.g., Delgado-Fernandez and Davidson-Arnott, 2011), attempts to relate regional wind records to local scale processes remains a significant challenge.

Our results indicate that down-scaling regional wind records with CFD could provide more representative turbulent boundary layer conditions, across multiple scales. For instance, this study was able to capture characteristic meso-scale airflow steering previously observed around Gran Canaria (Barton et al., 2000; Basterretxea et al., 2002) and flow velocity and directional perturbations at Maspalomas depending on the incident flow angle (Hernández-Calvento, 2006; Máyer-Suárez et al., 2012; Viera-Pérez, 2015). Simulated airflow velocity, directionality, and turbulence approaching the dunefield could then be used better predict processes operating at that scale or, provide incident boundary conditions to higher resolution meso- or micro-scale models. Similar approaches have been used successfully to down-scale wave models from global deep-water waves to intra-wave interactions operating in the nearshore (e.g., Guisado-Pintado, 2020). In this regard, modelling of aeolian environments could similarly adapt airflow conditions and include additional roughness elements and landforms, depending on the scale of interest; however, further studies are required to identify appropriate CFD model scaling practices for aeolian geomorphology.

It must be noted that the S-LES results presented in this study only account for the predominantly northerly wind conditions identified from the longest consistently recording regional meteorological station and, furthermore, does not account for additional airflow perturbations from dune landforms (Smith et al., 2017a), urbanization (Hernández-Calvento et al., 2014; Smith et al., 2017b), and other surface roughness features present at Maspalomas including vegetation (García-Romero et al., 2019b), 'goros' or human-built stone windbreakers (Peña-Alonso, 2015), and beach kiosks (Hernández-Calvento et al., 2002), or the potential contribution of diurnal winds (Máyer-Suárez et al., 2012). Given the generalizations of this meso-scale approach, it is beyond the scope of this current work to simulate all micro-scale airflow conditions at Maspalomas. Rather, this study demonstrates the utility of CFD to identify meso-scale airflow perturbations and the potential for scaling boundary conditions to better identify the dominant geomorphic drivers at multiple scales (de Boer, 1992). While the results of this work are unique to high profile island topography, magnifying the topographically steered flow around the coastline, a similar modelling approach can be considered in other regions that lack longer-term field measurements, have spatially and/or temporally limited regional meteorological data or in-situ measurements, have been modified by human development, and are located in areas of topographic complexity.

6. Conclusion

Transgressive dunefields around the Canary Islands have experienced rapid environmental changes largely since the 1970s, coinciding with a significant growth in tourism in the region (García-Romero et al., 2016). At Maspalomas, urban development has modified sediment transport pathways and airflow patterns across the dunefield (Hernández-Calvento et al., 2014; Smith et al., 2017b; García-Romero et al., 2019b). As a result, a dramatic increase in the areal coverage

and diversity of vegetation species in the urban shadow zone, expansion of deflationary slacks throughout the dunefield, and overall decrease in bare sand deposits has occurred since the 1960s (Hernández-Cordero et al., 2017, 2018; Smith et al., 2017b; García-Romero et al., 2019a, 2019b). Given the scale and rapidity of these changes occurring over the past 60 years, it is critical to improve our understanding of the aeolian processes that are responsible for the continual evolution of the environment.

Meso-scale airflow perturbations around Gran Canaria (Barton et al., 2000; Basterretxea et al., 2002) and at the Maspalomas dunefield (Nadal and Guitián, 1983; Martínez et al., 1986; Martínez, 1990; Naranjo, 1999; Hernández-Calvento, 2006; Hernández-Calvento et al., 2014; Máyer-Suárez et al., 2012; Viera-Pérez, 2015; Smith et al., 2017b; García-Romero et al., 2019b) have been previously observed and modelled. This study contributes to this knowledge by identifying spatiotemporal patterns of airflow perturbations and turbulent conditions that are capable of modifying sediment transport gradients at Maspalomas, during incremental changes to the incident northerly flow direction. Future studies could use these results to better predict aeolian dynamics at the dunefield-scale, or be used as inputs into smaller-scale CFD models that incorporates additional roughness elements and provides non-uniform sediment flux predictions across the dunefield. Furthermore, improving the predictions of airflow perturbations and sediment transport gradients could be used complimentary to existing management studies in the region, including the Arid Dune Vulnerability Index (ADVI) that integrates climatological, ecological, sedimentological, morphological, and anthropogenic data to assess the resiliency of beach-dune systems to environmental changes (Peña-Alonso et al., 2018). Lastly, a similar model approach could be used to simulate local wind conditions around other island topography, topographically complex aeolian environments, and where gaps or disparity in the regional wind records exist. The main conclusions are:

1. Simultaneous meteorological wind records from four sampled stations around Gran Canaria display significant variability, despite their relatively close proximity (i.e., within ~32 km). During our sample period, Aeropuerto and El Matorral recorded higher magnitude unimodal N-NNE winds, whereas decelerated bimodal conditions from the SW-NE developed at Inglés and Maspalomas. This suggests that topographic steering has a significant control on local airflow patterns around the coastline of Gran Canaria and that the use of meteorological data to describe the regional wind regime must be made in the context of larger scale airflow perturbations.
2. CFD simulations of northerly winds have identified two characteristic meso-scale airflow perturbations occurring around Gran Canaria, including: (1) Island-scale (i.e., 10s of km) bifurcation of airflow around the island steered parallel to the lateral coastlines before converging at the lee of the island, and (2) Smaller scale (i.e., ~2 km) turbulent canyon breezes that can further modify approaching airflow. The direction and magnitude of airflow perturbations depends on the sites position relative to the incident flow angle and topographic setting. At the Maspalomas dunefield, coherent turbulent flow structures were identified during simulations of North winds, resulting in highly variable instantaneous wind directions diverging up to 180° and velocities up to 47% higher than daily averages at Inglés and Maspalomas.
3. Remotely sensed observations of dune dynamics reveal variable patterns of migrations and directions and estimates of mass flux, developing between time series (i.e., t_1 and t_2) and within different sections of the dunefield. Furthermore, distinct signatures of bimodality including crest reversals and dunes with multiple slip faces were observed in t_2. These observations are inconsistent with unimodal wind conditions and sand drift potentials predicted over the entire study period. This suggests that regional wind conditions cannot adequately describe the local dunefield patterns at Maspalomas, without further consideration of localized airflow perturbations.
4. CFD can be used to simulate characteristic regional wind patterns and to identify the primary geomorphic drivers operating across aeolian environments. Maspalomas represents a distinct environment where airflow perturbations are occurring at a hierarchy of scales including individual dune landforms at the micro-scale, urbanization and canyon breezes at the meso-scale, and island-scale bifurcation of airflow around Gran Canaria. These results capture aeolian phenomena unique to Maspalomas; however, this study highlights the potential for using CFD to down-scale boundary layer conditions for areas with limited spatiotemporal wind records or in similarly complex wind environments.

CRediT authorship contribution statement

A. Smith – Conceptualization, Writing, Reviewing and Editing, Methodology, Formal Analysis.
D.W.T. Jackson – Conceptualization, Writing, Reviewing and Editing.
J.A.G. Cooper – Conceptualization, Writing, Reviewing and Editing.
M. Beyers – Conceptualization, Methodology, Reviewing and Editing.
C. Breen – Conceptualization, Reviewing and Editing.

Declaration of competing interest

The authors declare that they have no known competing financial interests or personal relationships that could have appeared to influence the work reported in this paper.

Acknowledgements

The authors would like to thank Luis Hernández-Calvento and the Universidad de Las Palmas de Gran Canaria (ULPGC) for providing resources and logistical support. Research funding was provided by a Ulster University Vice Chancellor's Research Scholarship (VCRS). This work is a contribution towards the project 'Caracterización de procesos socio-ecológicos de los sistemas playa-dunas de Canarias como base para su gestión sostenible', CSO2013-43256-R funded by the R&D+I (innovation) Spanish National Programme and a contribution to the UK Natural Environment Research Council grant NE/F019483/1.

References

Acosta, J, Uchupi, E., Muñoz, Herranz, P., Palomo, C., Ballesteros, M., ZEE Working Group. 2003. Geologic evolution of the Canarian Islands of Lanzarote, Fuerteventura, Gran Canaria and La Gomera and comparison of landslides at these islands with those at Tenerife, La alma and El Hierro. Mar. Geophys. Res. (24): 1–40.

Arens, S.M., 1996. Patterns of sand transport on vegetated foredunes. Geomorphology 17 (4), 339–350.

Baas, A.C.W., Jackson, D.W.T., Delgado-Fernandez, I., Lynch, K., Cooper, J.A.G., 2020. Using wind run to predict sand drift. Earth Surf. Process. Landf. 45 (8), 1817–1827.

Baddock, M.C., Wiggs, G.F.S., Livingstone, I., 2011. A field study of mean and turbulent flow characteristics upwind, over and downwind of barchans dunes. Earth Surf. Process. Landf. 36, 1435–1448.

Bagnold, R.A., 1941. The physics of wind-blown sand and desert dunes. Methuen, London 265 (10).

Barton, E.D., Basterretxea, G., Flament, P., Mitchelson-Jacob, E.G., Jones, B., Arístegui, J., Herrera, F., 2000. Lee region of Gran Canaria. J. Geophys. Res. 105, 17,173–17,193.

Basterretxea, G., Barton, E.D., Tett, P., Snagrá, P., Navarro-Perez, E., Arístegui, J., 2002. Eddy and deep chlorophyll maximum response to wind-shear in the lee of Gran Canaria. Deep-Sea Research I 49, 1087–1101.

Bauer, B.O., Davidson-Arnott, R.G.D., 2003. A general framework for modelling sediment supply to coastal dunes including wind angle, beach geometry and fetch effects. Geomorphology 49, 89–108.

Bauer, B.O., Davidson-Arnott, R.G., Walker, I.J., Hesp, P.A., Ollerhead, J., 2012. Wind direction and complex sediment transport response across a beach–dune system. Earth Surf. Process. Landf. 37 (15), 1661–1677.

Bauer, B.O., Walker, I.J., Baas, A.C.W., Jackson, D.W.T., Neuman, C.M., Wiggs, G.F.S. and Hesp, P.A. 2013. Critical Reflections on the Coherent Flow Structures Paradigm in Aeolian Geomorphology. Chap. 8 in. Venditti, J.G., Best, J.L., Church, M. and Hardy, R.J. (eds.) Coherent Flow Structures at Earth's Surface. Wiley-Blackwell. pp. 111–134. ISBN: 978-1-119-96277-9.

Beadnell, H.L. 1910. The Sand-Dunes of the Libyan Desert. Their origin, form, and rate of movement, considered in relation to the geological and meteorological conditions of the region. Geographical Journal: 379–392.

Belly, P.Y. 1964. Sand movement by wind U.S. Army Corps Eng. CERC. Tech. Mem. 1. Washington D.C. 38 pp.
Blocken, B., Stathopoulos, T., Carmeliet, J. 2007. CFD simulation of the atmospheric boundary layer: wall function problems. Atmospheric Environment (41-2): 238-252.
de Boer, D.H., 1992. Hierarchies and spatial scale in process geomorphology: a review. Geomorphology 4, 303–318.
Bourke, M., 2010. Barchan dune asymmetry: observations from Mars and Earth. Icarus 205, 183–197.
Bourke, M.C., Goudie, A.S., 2009. Varieties of barchan form in the Namib Desert and on Mars. Aeolian Res. 1, 45–54.
Bouzas, A.F., Alcántara-Carrió, J., Montes, I.M., Ojeda, A.B., Albarracín, S., de Rada, J.R.D., Salgado, J.R. 2013. Distribution and thickness of sedimentary facies in the coastal dune, beach, and nearshore sedimentary system at Maspalomas, Canary Islands. Geo-Marine Letters (33;2–3): 117–127.
Bullard, J.E., 1997. A note on the use of the "Fryberger method" for evaluating potential sand transport by wind. J. Sediment. Res. 67 (3), 499–501.
Bullard, J.E., Wiggs, G.F.S., Nash, D.J., 2000. Experimental study of wind directional variability in the vicinity of a model valley. Geomorphology 35, 127–143.
Chapman, C.A., Walker, I.J., Hesp, P.A., Bauer, B.O., Davidson-Arnott, R.G.D., 2012. Turbulent Reynolds stress and quadrant event activity in wind flow over a coastal foredune. Geomorphology 151-152, 1–12.
Chapman, C.A., Walker, I.J., Hesp, P.A., Bauer, B.O., Davidson-Arnott, R.G.D., Ollerhead, J., 2013. Reynolds stress and sand transport over a foredune. Earth Surface Landforms and Processes 38, 1735–1747.
Conover, J.H., 1964. The identification and significance of orographically induced clouds observe y TIROS satellites. J. Appl. Meteorol. 3, 226–234.
Cornwall, C., Bourke, M.C., Jackson, D.W.T., Cooper, J.A.G., 2018a. Aeolian slipface dynamics and grain flow morphologies on Earth and Mars. Icarus 314, 311–326.
Cornwall, C., Jackson, D.W.T., Bourke, M.C., Cooper, J.A.G., 2018b. Morphometric analysis of slip face processes of an aeolian dune: implications for grain-flow dynamics. Sedimentology 65 (6), 2034–2054.
Courant, R., Friedrichs, K., Lewy, H., 1928. Über die partiellen Differenzengleichungen der mathematischen Physik. Math. Ann. 100 (1), 32–74.
Delgado-Fernandez, I., 2010. A review of the application of the fetch effect to modelling sand supply to coastal foredunes. Aeolian Res. 2, 61–67.
Delgado-Fernandez, I., Davidson-Arnott, R.G.D., 2011. Meso-scale modelling of aeolian sediment input to coastal dunes. Geomorphology 130, 230–243.
Delgado-Fernandez, I., Jackson, D.W.T., Cooper, J.A.G., Baas, A.C.W., Lynch, K. and Beyers, M. 2011. Re-attachment zone characterisation under offshore winds blowing over complex foredune topography. Journal of Coastal Research (SI 64): 273-277.
Delgado-Fernandez, I., Davidson-Arnott, R.G.D., Bauer, B.O., Walker, I.J., Ollerhead, J., Rhew, H., 2012. Assessing aeolian beach-surface dynamics using a remote sensing approach. Earth Surf. Process. Landf. 37, 1651–1660.
Delgado-Fernandez, I., Jackson, D.W.T., Cooper, J.A.G., Baas, A.C.W., Beyers, J.H., Lynch, K., 2013a. Field characterization of three-dimensional lee-side airflow patterns under offshore winds at a beach-dune system. J. Geophys. Res. Earth Surf. 118, 706–721.
Delgado-Fernandez, I., Davidson-Arnott, R.G.D., Bauer, B.O., Walker, I.J., Ollerhead, J., 2013b. Evaluation of the optimal resolution for characterizing the effect of beach surface moisture derived from remote sensing on aeolian transport and deposition. J. Coast. Res. 2 (65), 1277–1282.
Delgado-Fernandez, I., Smyth, T.A.G., Jackson, D.W.T., Smith, A.B., Davidson-Arnott, R.G.D., 2018. Event-scale dynamics of a parabolic dune and its relevance for mesoscale evolution. Journal of Geophysical Research: Earth Surface 123 (11), 3084–3100.
Dong, P., 2015. Automated measurement of sand dune migration using multi-temporal lidar data and GIS. Int. J. Remote Sens. 36, 5426–5447.
Elbelrhiti, H., 2015. Field evidence of appearance and disappearance of the brink line on barchans. Aeolian Res. 18, 115–120.
Elbelrhiti, H., Douady, S., 2011. Equilibrium versus disequilibrium of barchan dunes. Geomorphology 125, 558–568.
Etling, D., 1989. On atmospheric vortex streets in the wake of large islands. Meteorog. Atmos. Phys. 41, 157–164.
Fernandopullé, D., 1976. Climatic Characteristics of the Canary Islands. Biogeography and ecology in the Canary Islands. Springer, Dordrecht, pp. 185–206.
Fryberger, S.G., Dean, G., 1979. Dune forms and wind regime. A Study of Global Sand Seas 1052, 137–169.
Funck, T., Schmincke, H.-U., 1998. Growth and destruction of Gran Canaria deduced from seismic reflection and bathymetric data. Journal of Geophysical Research: Solid Earth 103 (B7), 15393–15407.
García-Romero, L., Hernández-Cordero, A.I., Fernández-Cabrera, E., Peña-Alonso, C., Hernández-Calvento, L., Pérez-Chacón, E., 2016. Urban-Touristic Impacts on the Aeolian Sedimentary Systems of the Canary Islands: Conflict between Development and Conservation (Island Studies Journal).
García-Romero, L., Delgado-Fernández, I., Hesp, P.A., Hernández-Calvento, L., Hernández-Cordero, A.I., Viera-Pérez, M., 2019a. Biogeomorphological processes in an arid transgressive dunefield as indicators of human impact by urbanization. Sci. Total Environ. 650, 73–86.
García-Romero, L., Delgado-Fernández, I., Hesp, P.A., Hernández-Calvento, L., Viera-Pérez, M., Hernández-Cordero, A.I., Cabrera-Gámez, J., Domínguez-Brito, A.C., 2019b. Airflow dynamics, vegetation and aeolian erosive processes in a shadow zone leeward of a resort in an arid transgressive dune system. Aeolian Res. 38, 48–59.
Garvey, B., Castro, I.P, Wiggs, G., Bullard, J. 2005. Measurements of flows over isolated valleys. Boundary-layer meteorology (117-3): 417-446.
Gelaro, R., McCarty, W., Suárez, M.J., Todling, R., Molod, A., Takacs, L., Randles, C.A., Darmenov, A., Bosilovich, M.G., Reichle, R., Wargan, K., 2017. The modern-era retrospective analysis for research and applications, version 2 (MERRA-2). J. Clim. 30 (14), 5419–5454.
Guisado-Pintado, E., 2020. Shallow water wave modelling in the nearshore (SWAN). Sandy Beach Morphodynamics. Elsevier, pp. 391–419.
Heidorn, K.C., 1978. An index to measure consistency of the wind direction for periods around one day. Atmos. Environ. 12, 993–996.
Hellmann, G., 1916. Über die Bewegung der Luft in den untersten Schichten der Atmosphäre. Kgl. Akademie der Wissenschaften, Copenhagen, Denmark.
Hernández, L., Alonso, I., Ruiz, P., Pérez-Chacón, E., Suárez, C., Alcántar-Carrió, J. 2002. Decadal environmental changes on the dune field of Maspalomas (Canary Islands): evidences of an erosive tendency. In Littoral (Vol. 3, pp. 293-297).
Hernández, L., Alonso, I., Sánchez-Pérez, I., Alcántara-Carrió, J., Montesdeoca, I. 2007. Shortage of sediments in the Maspalomas dune field (gran Canaria, Canary Islands) deduced from the analysis of aerial photographs, foraminiferal content, and sediment transport trends. Journal of Coastal Research (23; 4): 993-999.
Hernández-Calvento, L., 2006. Diagnóstico sobre la evolución del sistema de dunas de Maspalomas (1960–2000). Cabildo Insular de Gran Canaria, Casa de Colón.
Hernández-Calvento, L., Ruis Flaño, P., Pérez-Chacón Espino, E., Suá Rodríguez, C., Alonso Bilbao, I., Alcántara-Carrió, J. 2002. Pasillos de sombra eólica generados pos los kioscos de Play del Ingés (Gran Canaria). Resultados Preliminares. Estudios recientes (2000—2002) en Geomortologia. Patrimonio, montara y dinamica tertitotial 2002. Dpto. Geografiá-UVA Valladolid, 141–148.
Hernández-Calvento, L. Jackson, D.W.T., Medina, R., Hernández-Cordero, Cruz, N., Requejo, S. 2014. Downwind effects on an arid dunefield from an evolving urbanised area. Aeolian Res. 15: 301–309.
Hernández-Cordero, A., Espino, E.P.C. and Calvento, L.H. 2006. Vegetation colonisation processes related to a reduction in sediment supply to the coastal dune field of Maspalomas (Gran Canaria, Canary Islands, Spain). Journal of Coastal Research, pp.69-76.
Hernández-Cordero, A., Romero, L.G., Hernández-Calvento, L., Espino, E.P.C., 2015. Tecnologías de la información geográfica aplicadas al análisis de la relación entre la vegetación y las tasas de desplazamiento de dunas en Maspalomas (Gran Canaria, Islas Canarias). Semata: Ciencias sociais e humanidades 27, 95–114.
Hernández-Cordero, A.I., Hernández-Calvento, L., Pérez-Chacón Espino, E., 2017. Vegetation changes as an indicator of impact from tourist development in an arid transgressive coastal dune field. Land Use Policy 64, 479–491.
Hernández-Cordero, A.I., Hernández-Calvento, L., Hesp, P.A., Pérez-Chacón, E., 2018. Geomorphological changes in an arid transgressive coastal dune field due to natural processes and human impacts. Earth Surf. Process. Landf. 43 (10), 2167–2180.
Hesp, P.A., Smyth, T.A., 2016. Jet flow over foredunes. Earth Surf. Process. Landf. 41 (12), 1727–1735.
Hesp, P.A., Smyth, T.A., 2019. CFD flow dynamics over model scarps and slopes. Physical Geography, pp. 1–24.
Hesp, P.A., Davidson-Arnott, R., Walker, I.J., Ollerhead, J., 2005. Flow dynamics over a foredune at Prince Edward Island, Canada. Geomorphology 65 (1–2), 71–84.
Hesp, P.A., Walker, I.J., Chapman, C., Davidson-Arnott, R., Bauer, B.O., et al., 2013. Aeolian dynamics over a coastal foredune, Prince Edward Island, Canada. Earth Surf. Process. Landf. 38 (13), 1566–1575. https://doi.org/10.1002/esp.3444.
Hesp, P.A., Smyth, T.A., Nielsen, P., Walker, I.J., Bauer, B.O., Davidson-Anott, R., 2015. Flow deflection over a foredune. Geomorphology 230, 64–74.
Jackson, P.S., Hunt, J.C.R., 1975. Turbulent wind flow over a low hill. Q. J. R. Meteorol. Soc. 101 (430), 929–955.
Jackson, D.W.T., Beyers, J.H.M., Lynch, K., Cooper, J.A.G., Baas, A.C.W., Delgado-Fernandez, I., 2011. Investigation of three-dimensional wind flow behaviour over coastal dune morphology under offshore winds using computational fluid dynamics (CFD) and ultrasonic anemometry. Earth Surf. Process. Landf. 36 (8), 1113–1124.
Jackson, D.W.T., Beyers, J.H.M., Delgado-Fernandez, I., Baas, A.C.W., Cooper, J.A.G., Lynch, K., 2013a. Airflow reversal and alternating corkscrew vortices in foredune wake zones during perpendicular and oblique offshore winds. Geomorphology 187, 86–93.
Jackson, D.W.T., Cruz-Avero, N., Smyth, T., Hernández-Calvento, L., 2013b. 3D airflow modelling and dune migration patterns in an arid coastal dune field. J. Coast. Res. Spec. Issue 65, 1301–1306.
Jackson, D.W.T., Cooper, J.A.G., Green, A., Beyers, M., Guisado-Pintado, E., Wiles, E., Benallack, K., Balme, M., 2020. Reversing transverse dunes: modelling of airflow switching using 3D computational fluid dynamics. Earth Planet. Sci. Lett. 544, 116363.
Jensen, N.O., Agee, E.M., 1978. Vortex cloud street during AMTEX 75. Tellus 30, 517–523.
Lee, Z.S., Baas, A.C.W., 2012. Streamline correction for the analysis of boundary layer turbulence. Geomorphology 171, 69–82.
Lettau, K., Lettau, H., 1978. Experimental and micrometeorological field studies of dune migration. In: Lettau, K., Lettau, H. (Eds.), Exploring the World's Driest Climate. Center for Climatic Research, University of Wisconsin-Madison, pp. 110–147, IES Report 101.
Lynch, K., Jackson, D.W., Cooper, J.A.G., 2010. Coastal foredune topography as a control on secondary airflow regimes under offshore winds. Earth Surface Processes and Landforms: The Journal of the British Geomorphological Research Group 35 (3), 344–353.
Madurapperuma, B., Lamping, J., McDermott, M., Murphy, B., McFarland, J., Deyoung, K., Smith, C., MacAdam, S., Monroe, S., Corro, L. and Magstadt, S., 2020. Factors Influencing Movement of the Manila Dunes and Its Impact on Establishing Non-Native Species. Remote Sensing, 12(10), p.1536.
Martínez, J., 1990. La provincia morfodinnámica de Morro Besudo- Faro de Masplomas (Isla de Gran Canaria, España): Conocimiento y comprensión de sus procesos geomorfológicos y sedimentarios para la planificación y gestión de este litoral. Reunión Nacional de Geomorfología 351–363.
Martínez, J., Carpio, P., Gómez, M., Hernández, T., Mena, A., 1986. Las dunas de Maspalomas: Geología e impacto del entorno. Excmo, Cabildo Insular de Gran Canaria.
Máyer-Suárez, P., Pérez-Chacón Espino, E., Cruz Avero, N., Hernández Calvento, L., 2012. Características del viento en el campo de dunas de Maspalomas (Gran Canaria, islas canarias, España). Nimbus 29-30, 281–397.

Nadal, I., Guitián, C., 1983. El sur de Gran Canaria: entre el turismo y la marginación. Cuadernos Canarios de Ciencias Sociales 9.
Naranjo, R. 1999. Maspalomas, escpacio natural. Concejalía de Turismo del Ayuntamiento de San Bartolomé de Tirajana, 365 pp.
Naya, A., 1984. Meteorología Superior. Espasa-Calpe, Madrid, pp. 1–546.
Nickling, W.G., Davidson-Arnott, R.G.D., 1990. Aeolian sediment transport on beaches and coastal sand dunes. National Research Council of, Canada, pp. 1–35.
Nordstrom, K.F., McCluskey, J.M., 1984. Considerations for control of house construction in coastal dunes. Coast. Manag. 12 (4), 385–402.
Nunalee, C.G., Basu, S. 2014. On the periodicity of atmospheric von Kármán vortex streets. Environmental Fluid Mechanics (14-6): 1335-1355.
Orlanski, I., 1975. A rational subdivision of scales for atmospheric processes. Bull. Am. Meteorol. Soc. 56 (5), 527–530.
Parsons, D.R., Wiggs, G.F., Walker, I.J., Ferguson, R.I., Garvey, B.G., 2004a. Numerical modelling of airflow over an idealised transverse dune. Environ. Model. Softw. 19 (2), 153–162.
Parsons, D.R., Walker, I.J., Wiggs, G.F., 2004b. Numerical modelling of flow structures over idealized transverse aeolian dunes of varying geometry. Geomorphology 59 (1–4), 149–164.
Parteli, E.J., Durán, O., Bourke, M.C., Tsoar, H., Pöschel, T., Herrmann, H., 2014. Origins of barchan dune asymmetry: insights from numerical simulations. Aeolian Res. 12, 121–133.
Parton, G., Dore, A., Vaughan, G., 2010. A climatology of mid-tropospheric mesoscale strong wind events as observed by the MST radar, Aberystwyth. Meteorol. Appl. 17, 340–354.
Pearce, K.I., Walker, I.J., 2005. Frequency and magnitude biases in the 'Fryberger' model, with implications for characterizing geomorphologically effective winds. Geomorphology 68, 39–55.
Pelletier, J.D., 2009. Controls on the height and spacing of eolian ripples and transverse dunes: a numerical modeling investigation. Geomorphology 105 (3–4), 322–333.
Peña-Alonso, C., 2015. Diseño y aplicación de indicadores de vulnerabilidad y calidad para playas y dunas de Canarias: una propuesta metodológica. PhD thesis. Universidad de las Palmas de Gran Canaria, 445 pp.
Peña-Alonso, C., Gallego-Fernández, J.B., Hernández-Calvento, L., Hernández-Cordero, A.I., Ariza, E., 2018. Assessing the geomorphological vulnerability of arid beach-dune systems. Sci. Total Environ. 635, 512–525.
Pérez-Chacón Espino, E., Hernández Calvento, L., Máyer-Suárez Suárez, P.L., Romero Martín, L.E., Alonso Bilbao, I., Mangas, J., Menéndez González, I., Sánchez Pérez, I., Ojeda Zújar, J., Ruiz Flaño, P., Alcántara Carrió, J., 2007. Maspalomas: claves científicas para el análisis de su problemática ambiental.
Savitzky, A., Golay, M.J., 1964. Smoothing and differentiation of data by simplified least squares procedures. Anal. Chem. 36 (8), 1627–1639.
Smagorinsky, J., 1963. General circulation experiments with the primitive equations: I. The basic experiment. Mon. Weather Rev. 91 (3), 99–164.
Smith, A.B., Jackson, D.W.T., Cooper, J., Andrew, G., 2017a. Three-dimensional airflow and sediment transport patterns over barchan dunes. Geomorphology 278, 28–42.
Smith, A., Jackson, D.W.T., Cooper, J.A.G., Hernández-Calvento, L., 2017b. Quantifying the role of urbanization on airflow perturbations and Dunefield evolution. Earth's Future 5 (5), 520–539.
Smith, A., Gares, P.A., Wasklewicz, T., Hesp, P.A., Walker, I.J., 2017c. Three years of morphologic changes at a bowl blowout, Cape Cod, USA. Geomorphology 295, 452–466.
Smyth, T.A.G., 2016. A review of computational fluid dynamics (CFD) airflow modelling over aeolian landforms. Aeolian Res. 22, 153–164.
Smyth, T.A.G., Jackson, D.W.T. and Cooper, J.A.G. 2012. High resolution measured and modelled three-dimensional airflow over a coastal bowl blowout. Geomorphology (177–178): 62–73.
Smyth, T.A.G., Jackson, D.W.T., Cooper, J.A.G., 2013. Three dimensional airflow patterns within a coastal trough-bowl blowout during fresh breeze to hurricane force winds. Aeolian Res. 9, 111–123.
Smyth, T.A.G., Jackson, D.W.T., Cooper, J.A.G., 2014. Airflow and aeolian sediment transport patterns within a coastal trough blowout during lateral wind conditions. Earth Surf. Process. Landf. 39, 1847–1854.
Smyth, T.A.G., Hesp, P.A., Walker, I.J., Wasklewicz, T., Gares, P.A., Smith, A.B., 2019. Topographic change and numerically modelled near surface wind flow in a bowl blowout. Earth Surf. Process. Landf. https://doi.org/10.1002/esp.4625.
Smyth, T.A.G., Delgado-Fernandez, I., Jackson, D.W.T., Yurk, B., Rooney, P., 2020. Greedy Parabolics: Wind Flow Direction within the Deflation Basin of Parabolic Dunes Is Governed by Deflation Basin Width and Depth. Progress in Physical. Earth and Environment, Geography https://doi.org/10.1177/0309133319899306.
Troen, I., Petersen, E.L., 1989. European wind atlas. Roskilde: Riso National Laboratory 1989, 1.
Tsoar, H. 1985. Profiles Analysis of sand Dunes and Their Steady State Signification. Geografiska Annaler (67 A): 47–58.
Vallejo, I., Hernández Calvento, L., Ojeda, J., Mayer, P., Gómez Molina, A., 2009. Caracterización morfométrica y balance sedimentario en el Sistema de dunas de Maspalomas (Gran Canaria) a partir de datos LIDAR. Rev. Soc. Geol. Esp. 22 (1–2), 57–65.
Van Driest, E.R., 1956. On turbulent flow near a wall. Journal of the aeronautical sciences 23 (11), 1007–1011.
Viera-Pérez, M., 2015. Estudio detallado de la duna costera de Maspalomas (Gran Canaria, Islas Canarias): interacción" Taganum moquinii"-dinámica sedimentaria eólica en un entorno intervenido. Recomendaciones de cara a su gestión Universidad de Las Palmas de Gran Canaria. 570 pp.
Walker, I.J., 1999. Secondary airflow and sediment transport in the lee of a reversing dune. Earth Surface Processes and Landforms: The Journal of the British Geomorphological Research Group 24 (5), 437–448.
Walker, I.J., Davidson-Arnott, R.G.B., Bauer, B.O., Hesp, P.A., Delgado-Fernadez, I., Ollerhead, J., Smyth, T.A.G., 2018. Scale-dependent perspectives on the geomorphology and evolution of beach-dune systems. Earth Sci. Rev. 171, 220–253.
Wasson, R.J., Hyde, R., 1983. Factors determining desert dune type. Nature 304 (5924), 337–339.
Weaver, C.M., Wiggs, G.F.S., 2011. Field measurements of mean and turbulent airflow over a barchans sand dune. Geomorphology 128, 32–41.
Wiggs, G.F.S. and Weaver, C.M. 2012. Turbulent flow structures and aeolian sediment transport over a barchan sand dune. Geophysical Research Letters (39): (L05404).
Wiggs, G.F.S., Bullard, J.E., Garvey, B., Castro, I., 2002. Interactions between airflow and valley topography with implications for Aeolian sediment transport. Phys. Geogr. 23, 366–380.
Wilson, I.G., 1972. Aeolian bedforms – their development and origins. Sedimentology 19, 173–210.
Zhao, Y., Gao, X., Lei, J., Li, S., Cai, D., Song, Q., 2019. Effects of wind velocity and Nebkha geometry on shadow dune formation. Journal of Geophysical Research: Earth Surface 124 (11), 2579–2601.
Zimmerman, L.I., 1969. Atmospheric wake phenomena near the Canary Islands. J. Appl. Meteorol. 8, 896–907.